

Geochemistry and Petrology of the most Recent Deposits from Cotopaxi Volcano, Northern Volcanic Zone, Ecuador

GARRISON, JENNIFER M., DAVIDSON, JON P., HALL, MINARD, MOTHES,
PATRICIA

ABSTRACT

Cotopaxi volcano is located in the Northern Volcanic Zone (NVZ) of the South American Andes. Pyroclastic deposits and lava flows from Cotopaxi comprise basaltic andesites, andesites and rhyolites that have erupted since 13,200 years ago. Nine rhyolite eruptions were produced in at least five separate events, punctuated by intermittent andesite eruptions. High La/Yb (>5) and ^{230}Th excesses in the andesites are consistent with equilibration of magma with garnet-bearing lower crust or mantle, and numerical models show that lower crustal AFC involving crystallization of amphibole and plagioclase is sufficient to create the observed variations in the trace elements. The Cotopaxi andesites contain glomerocrysts of plagioclase + pyroxene, and at least four populations of plagioclase crystals indicate pervasive magma mixing. Sr, Nd and Pb isotopes are consistent with 5-20 % assimilation of radiogenic crust, but higher levels of mafic crust (cryptic assimilation) and/or source contamination by volcanogenic sediments are also likely. The Cotopaxi rhyolites formed from compaction and extraction of high-SiO₂ melt from an andesitic crystal mush. On the basis of U-series data, the residence time of the rhyolites is on the order of 74,000 years. Temporal variations in MgO and Sr of the Cotopaxi andesites reflect frequent recharge of the Cotopaxi system, variable recharge composition and a system that has not become more evolved over time.

INTRODUCTION

Studies of individual arc volcanoes reveal clues about process timescales, recycling of crust and, ultimately, formation of continents. Cotopaxi Volcano is one of the more well-known volcanoes in South America, and from a geochemical perspective it provides an ideal opportunity to learn about the intricate details of the sub-volcanic magma system.

Well-exposed lava flows and pyroclastic deposits allow for detailed examination of volcanic deposits, and the stratigraphy has been well documented and calibrated by Hall and Mothes (2008). Cotopaxi has the unusual characteristic of producing both rhyolite

and andesite eruptions, and the combination of this geochemical variation and calibrated stratigraphy provide a powerful tool for learning about petrogenesis in Ecuador over the past 13.2 ka. Our data reveal a particularly rich record including recycling of the 2.1 Ga old South American craton, repeated recharge by several andesitic magmas and the formation of rhyolite by compaction and melt extraction from andesitic crystal mush. The overarching goal of this paper is to present a petrogenetic model for the compositional variation at Cotopaxi Volcano that takes into account the geochemical and temporal variation in the Cotopaxi andesites and rhyolites.

Geologic setting

The Northern Volcanic Zone (NVZ) of the Andes ($5^{\circ}\text{N} - 2^{\circ}\text{S}$) is the northernmost of three active volcanic zones in South America (Fig. 1a) formed by eastward subduction of the Nazca Plate beneath the South American Plate (Lonsdale, 1978). The dip of the slab is estimated to be $25\text{-}35^{\circ}$ (Guillier et al., 2001, Taboada et al., 2000) and the depth to the slab beneath the arc front is estimated to be 100-150 km (Taboada et al., 2000). Volcanoes in Ecuador are distributed between two parallel mountain ranges, the Eastern and Western Cordillera (Fig. 1b), that are separated by an extensional basin called the Interandean Depression (Spikings et al., 2005). Cotopaxi Volcano ($1^{\circ}15'\text{S}, 78^{\circ}25'\text{W}$) is located in the Eastern Cordillera, approximately 60 km south of the capital city of Quito. Crustal thickness in the NVZ ranges from ~ 20 km near the coast to approximately 70 km beneath the Cordillera; in fact the lowest gravity anomaly in the entire Andean arc (-292 mgal) is beneath the NVZ (Feininger and Seguin, 1983). The crust beneath the Eastern Cordillera and the Interandean Depression consist of accreted felsic terrains and plutons that crop out

as narrow belts extending northward into Colombia (McCourt et al., 1984). Accreted oceanic plateau and island arc terrains, collectively referred to as the Northern Andean Block (NAB), comprise the basement beneath the Western Cordillera (Spikings, et al., 2005, Mamberti et al., 2003, Hughes and Pilatasig, 2002). In southwestern Ecuador, exhumed high-grade metamorphic rocks of the Raspas Metamorphic Complex (Fig. 1b) record pressures of \sim 2.0 GPa and temperatures of 600° C, and may be representative of the basement beneath Ecuador (Bosch et al., 2002, Arculus et al., 1999; Feininger, 1980).

The most recent eruption of Cotopaxi occurred in 1877 (Wolf, 1878), and fumarolic activity on the flanks and summit of Cotopaxi suggests that there is ongoing subvolcanic magmatic activity. Since 1534 Cotopaxi has experienced at least 13 andesitic eruptions (Hall and Mothes, 2008) that range from effusive lava flows to explosive strombolian and plinian style plumes. Eruptions are characterized by high eruptive power and column heights of 28-39 km (Barberi et al., 1995), with estimated volumes of 0.01 – 8 km³. Sector collapse, debris avalanches, lahars and pyroclastic flow deposits are also associated with past activity at Cotopaxi, and still pose significant hazards to surrounding communities (Mothes et al., 2004, Mothes et al., 1998, Mothes, 1992).

Stratigraphy

The Cotopaxi deposits consist of an older section, called Cotopaxi I, and a younger section called Cotopaxi II (Hall and Mothes, 2008) (Fig. 2a). The Cotopaxi I deposits include a series of rhyolitic pyroclastic flow and ash falls that range from 420-560 kyr old (fission track ages; Bigazzi et al, 1997), and are collectively called the Barrancas Sequence. These ignimbrites represent the 32 km³ explosive eruption of the Cotopaxi

Caldera, the remnant of which forms an arcuate edifice that has an estimated diameter of 8 km (Hall and Mothes, 2008). To the southeast of Cotopaxi is the Chalupas Caldera (Fig. 1c), a 12-km diameter caldera that produced the Chalupas Ignimbrite 211 kyr ago (Hammersley and DePaolo, 2003, Hall and Mothes, 2008). This ignimbrite caps the Barrancas Sequence (Hall and Mothes, 2008). A 150 ka old glacial till deposit separates the Cotopaxi I and Chalupas Ignimbrite from the younger Cotopaxi II sequence that ranges in age from 13.2 ka to 1877 AD (Hall and Mothes, 2008). Lava flows related to a satellite vent on Cotopaxi, called the Morurcu vent (Fig. 1c), are found in conjunction with the glacial till deposit, and are therefore inferred to be older than 13.2 ka old, but younger than 211 ka (Hall and Mothes, 2008). This paper focuses on the Cotopaxi II sequence.

The Cotopaxi II sequence is subdivided into the Cotopaxi IIA (lower) and Cotopaxi IIB (upper) units; each contains pyroclastic deposits of andesite and rhyolite (Fig. 2b,c). The oldest Cotopaxi IIA deposits are collectively called the F-rhyolite series (Hall and Mothes, 2008), and comprise seven individual ash fall and pyroclastic flow deposits. Two other rhyolite eruptions at 7.2 ka and 6.3 ka are separated from the F-series rhyolites by thick deposits of andesite scoria and lava flows. The Cotopaxi IIB section comprises a series of andesitic scoria falls, lava flows and a single rhyolite eruption. The unit that separates the Cotopaxi IIA section from the Cotopaxi IIB deposits is the Colorado Canyon Ignimbrite, a 4500 year old pyroclastic flow that is well exposed on the north flank of Cotopaxi in an incised valley called the Colorado Canyon. On the basis of location and stratigraphy, this ignimbrite was presumed to have erupted from Cotopaxi Volcano, however the Colorado Canyon Ignimbrite is geochemically and isotopically more similar to the 211 kyr old Chalupas Caldera Ignimbrite than to the Cotopaxi rhyolites (Fig. 2b,c).

Following the Colorado Canyon eruption, Cotopaxi produced andesite (the Cotopaxi IIB series), and the Peñas Blancas rhyolite, which erupted 2200 years ago and has a composition that is consistent with the Cotopaxi rhyolites.

Widely dispersed pyroclastic deposits and lava flows, well-preserved stratigraphic exposures and an extensive, accessible ring plain allow for sampling around nearly the entire Cotopaxi cone, making it ideal for this stratigraphically-controlled study. The exposures of pyroclastic deposits at Cotopaxi, which include several distinctive marker units, allow for a well-constrained volcanic stratigraphy. One consequence of the highly porous nature of vesicular pyroclasts is the increased likelihood of alteration due to weathering, but leached and unleached samples were not significantly different in terms of major elements, trace elements or Sr isotopes. We therefore conclude that weathering has minimal effects on rock compositions and on the outcome of this study (see Analytical Methods). Reasons for the limited alteration may be the combination of altitude, temperature and precipitation; the ring plain of Cotopaxi is above 3630 m, and although it is cold for most of the year, the amount of annual precipitation is a fraction of what it is at lower elevations in the Amazon Basin.

ANALYTICAL METHODS

A total of 76 samples from lava flows and pyroclastic fall deposits were used for this study, collected from the flanks and ring plain of Cotopaxi, including 22 units from Cotopaxi IIA, 46 units from Cotopaxi IIB, 5 samples of the Colorado Canyon Ignimbrite and rhyolite from the Chalupas Caldera (Fig. A1). Metamorphic basement samples of greenschist and mica schist were collected east of the Eastern Cordillera at the Guadalupe

Volcanic Observatory near Tungurahua Volcano along with three samples from the Morurcu satellite vent lavas.

All samples were ground in a ceramic shatterbox and analyzed for major and trace elements (data in Table 1) using ICPMS/XRF at Washington State University's GeoAnalytical Laboratory in Pullman, Washington using analytical techniques outlined in Knaack et al. (1994) and Johnson et al (1999). Accuracy was determined using the standard values for AGV-1 and G-2. Precision was determined using internal standards BCR-P and GSP-1, and is better than 1% for the major elements, 5% for the REEs and 10 % for the other trace elements. A representative subgroup of samples was chosen for $^{87}\text{Sr}/^{86}\text{Sr}$ ($n=50$), $^{143}\text{Nd}/^{144}\text{Nd}$ ($n=38$) and $^{206}\text{Pb}/^{204}\text{Pb}$, $^{207}\text{Pb}/^{204}\text{Pb}$, $^{208}\text{Pb}/^{204}\text{Pb}$ ($n=16$) analyses (Table 2), which were conducted on a VG Sector thermal ionization mass spectrometer (TIMS) at the W.M. Keck Center for Isotope Geochemistry at UCLA. Accuracy was monitored using standards, for which we determined $^{87}\text{Sr}/^{86}\text{Sr} = 0.710258 \pm 10$ for NBS-987 ($n = 14$), $^{143}\text{Nd}/^{144}\text{Nd} = 0.511852 \pm 12$ for La Jolla ($N = 10$). Pb isotope fractionation correction was achieved by determining the value for the NBS 981 standard relative to the accepted value of 16.937 ± 12 for $^{206}\text{Pb}/^{204}\text{Pb}$ ($n = 6$), 15.491 ± 12 for $^{207}\text{Pb}/^{204}\text{Pb}$, and 36.549 ± 12 for $^{208}\text{Pb}/^{204}\text{Pb}$ resulting in fraction corrections of 266, 301 and 321 ppm, respectively.

Meticulous removal of weathering rinds during sample processing helped minimize the effect of alteration. In order to determine the effects of weathering on the pyroclastic rocks, a group of samples representing various compositions were leached for several hours in dilute nitric acid prior to analysis. After leaching, the leached and non-leached samples (designated as *a* and *b* in Table 1) were dried and prepared for analysis. There was

no significant difference between leached and unleached samples, and we are confident that magmatic compositions have not been compromised by weathering.

U-series isotopes (U and Th) for whole rocks and mineral separates were analyzed at Bristol University (analytical details in Garrison et al., 2006). Minerals for oxygen isotope analysis (Table 3) were separated using heavy liquids, leached in dilute hydrofluoric acid, then hand-picked to ~98 % purity. Oxygen isotopes were measured for two rhyolites (CTX-17 and 19) and three andesites (CTX-25, 26 and 129) using the Optima mass spectrometer at Royal Holloway University of London, using the Gore Mountain Garnet (GMG) as a standard ($\delta^{18}\text{O} = 5.78 \pm 0.2$).

Zircon crystals were separated from the most evolved Cotopaxi rhyolite (CTX-17, n = 7) and from the Chalupas Caldera rhyolite (n = 12) and analyzed for U-Pb ages using the method of Dalyrmple et al. (1999) and the AS-3 standard. All zircon analyses were carried out using the Cameca IMS 1270 ion microprobe at the W.M. Keck Center for Isotope Geochemistry at UCLA. Prior to analyses, zoning in the grains was imaged using a LEO 1430VP scanning electron microscope cathodoluminescence (CL) detector, also at UCLA. Modal abundances of minerals in thin section were determined by point counting. Mineral and glass compositions were measured using the JEOL JXA-8200 electron microprobe at UCLA. Mineral data are given in Table A1. Further details of sample locations and preparation are given in Garrison (2004).

RESULTS

Petrography

The Cotopaxi II lava flows (referred to as lavas A, B and D in Hall and Mothes, 2008) contain 48-23% crystals; the groundmass contains abundant microphenocrysts of plagioclase that give rise to trachytic textures. Of the phenocrysts, plagioclase comprises 80-85 %; clinopyroxene and orthopyroxene phenocrysts account for roughly equal percentages of 7-10 % each (Fig. A2). Accessory ilmenite and magnetite comprise ~ 1% of the lavas. The scoria clasts range from moderately to highly vesicular (25-60 % vesicles) and contain 70-92 modal % groundmass, including microphenocrysts of plagioclase. Plagioclase also comprises 75-90 % of the phenocryst population, whereas 10-20 % of the phenocrysts are orthopyroxene that decrease with increasing SiO₂ content (Fig. A2). Clinopyroxene comprises the remaining 8-20 %, and the abundance is positively correlated with wt % SiO₂. At least four populations of plagioclase phenocrysts are observed in the lavas and pyroclastic deposits; those with resorbed cores, resorbed rims, whole crystal resorption and no resorption (pristine crystals) (Fig. 3a-d). Melt inclusions are observed in many plagioclase crystals (Fig. 3e). All of the analyzed mafic rocks contain clinopyroxene and orthopyroxene, either as intergrowths (Fig. 3f) or as pristine crystals (Fig. 4a,b). Olivine is found as inclusions in the orthopyroxene. (Fig 4c). The Morurcu lavas contain ~ 25-48 % crystals, primarily amphibole and plagioclase, with sparse clinopyroxene. The amphibole in the Morurcu samples is severely resorbed and does not appear to be in equilibrium with the groundmass (Fig. 4d).

The Cotopaxi rhyolites are aphyric and contain only 2-4 % phenocrysts, including plagioclase, biotite, amphibole and trace amounts of quartz, oxides, apatite, alanite and

zircon. Unlike the plagioclase crystals from the andesites, the rhyolite plagioclase crystals are pristine, show normal zonation and are commonly broken (Fig. 4e). The pyroclastic flow deposits contain obsidian and volcanic lithics in the matrix, and the pumice clasts are white, fairly dense and non-fibrous. This in contrast to pumice clasts from the Chalupas Ignimbrite that are gray in color, glassy, highly fibrous and contain 1-2% plagioclase and biotite crystals, with accessory apatite and oxides. The Colorado Canyon rhyolite pumices have the same texture and mineralogy as the Cotopaxi rhyolite. Amphibole is observed in only the least evolved rhyolite; they are pristine and lack alteration rims (Fig. 4f).

Plagioclase crystals from the Cotopaxi rhyolite range in composition from An₂₇-An₅₂, whereas plagioclase crystals in the andesites range from An₅₀-An₈₀ (Fig. 5a, Table A1), with no consistent relation between core and rim compositions. Clinopyroxene crystals that are found in some of the rhyolites have the same composition as clinopyroxene found in the andesites (Fig. 5b).

Geochemistry

Major and trace elements

Major and trace element data are presented in Table 1. The Cotopaxi samples comprise medium K₂O basaltic andesites, andesites and rhyolites, and the Chalupas and Colorado Canyon Ignimbrites are high-K₂O rhyolites (Fig. 2b). Major elements define differentiation trends that are characteristic of subduction-related volcanic rocks; the basaltic andesites and andesites show decreasing FeO, MgO (Fig. 2c), CaO, Al₂O₃ and TiO₂ with increasing SiO₂ that typically reflects fractionation of plagioclase + pyroxene + oxides ± olivine. K₂O and Na₂O are positively correlated with SiO₂. The SiO₂ content of

glass in the andesite groundmass ranges from 61-78 %, higher than the correlative andesite whole rocks (55-60 wt %), and the K₂O content of the andesite glass ranges from 1.5-3.0 wt %, compared to the whole rock values from 1.2-1.8 wt % (Fig. 6, Table A1). The Cotopaxi rhyolites have higher concentrations of K₂O (Fig. 2b) and Na₂O than the andesites, and P₂O₅ is negatively correlated with SiO₂ content. The rhyolite glass contains 72-76 wt % SiO₂, 1-3 wt % higher than the rhyolite whole rocks, whereas the K₂O content in the rhyolite glass is 1.9-2.7 wt % lower than in the whole rocks (Fig. 6).

Incompatible trace element (ITE) and rare earth element (REE) diagrams for the Cotopaxi rocks are shown in Fig. 7a-c. All samples show characteristics that are typical of subduction zone volcanic rocks, including relative Ta-Nb depletions and enrichment in the large ion lithophile and light rare earth elements (LILE, LREE) compared to the heavy rare earth elements (HREE). The Ta-Nb depletion in arc lavas is presumed to be a characteristic of the source and that reflects the relatively low fluid mobility of Ta and Nb (Schmidt et al., 2004), or alternatively, the sequestering of Ta and Nb in a residual mantle phase (Tiepolo et al., 2000). The enrichment in the LILE and LREE concentrations, including K, U, Sr, Ba, Th, Pb and La is attributed to the slab fluid component as well as to the relative incompatibility of these elements during crystallization (Hawkesworth et al., 1997, Davdison, 1986). Relative depletions in the REE are commonly illustrated using LREE/HREE (Fig. 7c), specifically La/Yb or La/Lu. Values of La/Yb > 5 are considered to be fractionated, and the Cotopaxi andesites range from 7-19 in the andesites and 25-35 in the rhyolites. Similarly, fractionation between the LREE and MREE is shown using La/Dy, and values are lower in the andesites (4-8) than in the rhyolites (12-16). The Ni concentrations range from 13-51 ppm in the basaltic andesites to 3-36 ppm in the andesites

and 1-11 ppm in the rhyolites. The rhyolites are similar to the andesites, but are depleted with respect to P, Ti, MREE and HREE concentrations, and have higher concentrations of the LILE, LREE, Ta and Nb. Ta/Nb ratios in the rhyolites range from 0.08-01, compared to the andesites that have constant Ta/Nb of 0.07. This observed variation correlates with a decrease in Sr concentrations between the andesites (480-695) and the rhyolites (220-320 ppm).

Isotopes

Sr, Nd, and Pb isotopic compositions for the Cotopaxi samples are listed in Table 2. The Cotopaxi andesites and basaltic andesites have $^{87}\text{Sr}/^{86}\text{Sr}$ and $^{143}\text{Nd}/^{144}\text{Nd}$ that overlap with the rhyolite values (Fig. 8a inset). The average NVZ $^{87}\text{Sr}/^{86}\text{Sr}$ value of 0.70420 is only slightly higher than the Cotopaxi average of 0.70418. The Cotopaxi data are broadly similar to values for the accreted mafic terrain (Mamberti et al., 2003), volcanic rocks of the NVZ (Bryant et al., 2006, Barragan et al., 1998, Harmon, 1984) and have lower $^{143}\text{Nd}/^{144}\text{Nd}$ than the Raspas Terrain (Bosch et al., 2002) and MORB. Cotopaxi $^{87}\text{Sr}/^{86}\text{Sr}$ values are slightly higher than MORB and the Galapagos OIB (White et al., 1993). The Chalupas Caldera and Colorado Canyon samples have higher $^{87}\text{Sr}/^{86}\text{Sr}$ than the Cotopaxi samples.

The range in Pb isotope values for the Cotopaxi samples corresponds closely to the relatively narrow range of Pb isotope data from other NVZ volcanoes and accreted terrain reported by Bryant et al. (2006), Chiaradia et al. (2009) and Harmon (1984) (Fig. 8b). Values for the Cotopaxi andesites overlaps that of the rhyolites; the Colorado Canyon Ignimbrite has higher $^{207}\text{Pb}/^{204}\text{Pb}$ that is very similar to the Chalupas rhyolite. The greenschist facies basement sample has lower $^{207}\text{Pb}/^{204}\text{Pb}$ and the same $^{206}\text{Pb}/^{204}\text{Pb}$ as the

Cotopaxi andesites. Together, these data form a linear trend on a $^{207}\text{Pb}/^{204}\text{Pb}$ versus $^{206}\text{Pb}/^{204}\text{Pb}$ diagram that extends from Ecuadorian crust values (Raspas metapelite, Bosch et al., 2002) to Nazca Plate MORB and Galapagos OIB (Fig. 8b).

U-series isotopes (^{238}U - ^{230}Th) were measured on mineral separates and whole rocks from Cotopaxi, and have been previously published as part of a study to link the degree of U-series disequilibria in arc volcanic rocks to crustal thickness, a parameter that may exert some control over processes that fractionate U from Th (Garrison et al., 2006). U-series data are typically represented as activity ratios that relate to the degree of equilibrium between (^{230}Th) and (^{238}U), and are also used to extract age information that relates to the time required for the system to return to equilibrium (Bourdon et al., 2000, Hawkesworth et al., 2004, 2000, 1997). Any activity ratio other than unity signifies fractionation of U from Th within the last 350 ka. The ($^{238}\text{U}/^{230}\text{Th}$) for the Cotopaxi andesite whole rocks range from 0.96 – 1.07 and the ($^{238}\text{U}/^{230}\text{Th}$) of the rhyolite whole rocks ranges from 1.03-1.14 (i.e. 3-14 % excess ^{238}U) (Fig. 9a). The ^{230}Th excesses in the andesites are attributed to mixing of arc magma with a 3-20% lower crustal eclogite melt, whereas the ^{238}U excesses in the Cotopaxi rhyolites are explained by fractionation of accessory alanite and apatite 74,000 years ago during rhyolite formation (Fig. 9c) (Garrison et al., 2006). The overall conclusion from these data is that differentiation processes, rather than exclusively source processes, can control the partitioning of U and Th isotopes in continental arcs, and in evolved rocks, accessory phases such as alanite, apatite and zircon can create large ^{238}U or ^{230}Th excesses. A summary of this model is shown in Fig. 9c.

Whole rock $\delta^{18}\text{O}$ values are listed in Table 3, and mineral-mineral equilibrium temperatures are shown in Fig. A4. Mineral values vary from $6.42 - 8.27 (\pm 0.42) \text{ ‰}$ in the rhyolites, and from $6.49 - 6.93 (\pm 0.42) \text{ ‰}$ in the andesites. The andesite glass has $\delta^{18}\text{O} > \text{whole rock}$, however on the basis of resorption and mixing textures, it is likely that some of the minerals are not in equilibrium with the glass in the andesites. Pristine textures of the minerals in the rhyolite indicate that they are likely in equilibrium and thus the rhyolite glass-mineral pairs give more realistic magmatic temperatures (Wolff and Balsley, 2002). Calculated glass-mineral $\delta^{18}\text{O}$ temperatures range from $700-1400^\circ\text{C}$ in the andesites and $470-900^\circ\text{C}$ in the rhyolites.

DISCUSSION

Source versus differentiation processes in the Cotopaxi andesites

In general, the sub-arc mantle source of arc magmas is thought to be imprinted with sediment and fluid signatures from the subducting lithosphere (Turner et al., 2000, Peacock, 1990). The sediment signature is in part a function of eroded forearc crust (Plank and Langmuir, 1998), and in the NVZ this is likely to be juvenile volcanogenic rock from the accreted oceanic plateau (Mamberti, 2005) and/or the Macuchi island arc terrain (Chiardia et al., 2009). The similarities in isotopic composition between these terrains, MORB and the Cotopaxi data, particularly with respect to $^{207}\text{Pb}/^{204}\text{Pb}$ (Fig. 8b), make it difficult to assess the effect of sediment subduction on the composition of the Cotopaxi lavas. A graph of $^{87}\text{Sr}/^{86}\text{Sr}$ versus $\delta^{18}\text{O}$ shows that crustal contamination is predominant over source contamination in this system (Fig. 10); this is modeled using a crustal $^{87}\text{Sr}/^{86}\text{Sr}$ value for metapelitic schist of the Raspas terrain (Bosch et al., 2002). The slab fluid

signature, as identified by relative enrichments in the LILE is clearly apparent in the Cotopaxi magmas, despite the lack of ^{238}U excesses in the andesites (Garrison et al., 2006) that is typically associated with fluid addition (Turner et al., 2000). One explanation for this is that the lower crustal melting process overprints the fluid signature at Cotopaxi (Garrison et al., 2006), a process also documented at Parinacota volcano in the CVZ (Hora et al., 2009).

In terms of differentiation processes at Cotopaxi, trace element data are consistent with lower crustal assimilation and fractional crystallization (AFC) processes, followed by magma mixing and mid-upper crustal AFC. The Cotopaxi U-series data are modeled using a 3-20 % melt of garnet amphibolite as the assimilant in primitive magma (Garrison et al., 2006). We use the Raspas Terrain metapelitic schist as the assimilant in models of isotope variation in this paper (Bosch et al., 2002), for the reason that it is a much better fit to the Cotopaxi data. The range in $^{87}\text{Sr}/^{86}\text{Sr}$ and $^{143}\text{Nd}/^{144}\text{Nd}$ isotope variation cannot be reproduced using the isotope values of the accreted terrain or the Raspas garnet amphibolite (Fig. 8a,b). The AFC model in Fig. 11b shows the range of La/Yb and Sr values that are generated by a mixture of arc basalt (Mt Shasta basalts, Baker et al., 1994) with a 7- 15 % partial melt of lower crust. The range of mixtures (shaded region on Fig. 11b) is a reasonable fit to the Cotopaxi data. The isotope variation is also consistent with this model; the shift in the Cotopaxi data toward higher $^{143}\text{Nd}/^{144}\text{Nd}$ ratios is consistent with 10-20 % assimilation of metapelitic crust (Fig. 8a). The $^{207}\text{Pb}/^{204}\text{Pb}$ values of the accreted NAB terrain span the entire range from MORB to Ecuadorian crust, however the Cotopaxi data can be explained using a 5-15 % mixture of metapelite with MORB (Fig. 8b). In addition to consistently reproducing the isotope variation in the Cotopaxi rocks,

the metapelitic schist is more likely to be the source of Precambrian zircon in the Cotopaxi rocks than the mafic garnet amphibolite used by Garrison et al. (2006).

Crystal fractionation in the andesites was modeled using olivine, clinopyroxene, orthopyroxene, plagioclase and amphibole. Although amphibole is not observed in thin section, the La/Dy and Sr concentrations cannot be reproduced without amphibole in the crystallizing assemblage (Fig. 11a). Phase equilibria experiments show that amphibole is the dominant phase from 0.7-1.2 GPa (Alonso-Perez et al., 2009), consistent with studies of amphibole-rich inclusions found in arc lavas (e.g. Merapi, Chadwick et al., 2010) and plutons (Larocque, J. and Cani, 2009). A fractionating assemblage of amphibole (30%) + plagioclase (14 %) + clinopyroxene (20%) + orthopyroxene (20%) + olivine (16%) reproduces the trend in the Cotopaxi andesites over a range of 10 – 50% crystallization ($F = 0.9\text{--}0.5$). The low rate of plagioclase crystallization is not uncommon in arcs, and is believed to be caused by the high P_{H_2O} of arc magmas that causes suppression of plagioclase at lower crustal depths (Danyushevsky, 2001). Interestingly, the amphibole-bearing Morurcu andesites have Sr concentrations that decrease in tandem with La/Dy, consistent with the re-incorporation of MREE into the melt as amphibole becomes unstable at shallower depths. The highly resorbed texture of the Morurcu crystals (Fig. 4d) indicates that amphibole was initially stable and dissolved during ascent (Davidson et al., 2007, Ribeiro-Lauret, 2008).

Changes in pressure and temperature during magma ascent and storage are evident in the mineral textures. Inclusions of olivine in the basaltic andesite orthopyroxene (Fig. 4c) indicate that olivine was an early crystallizing phase, and pristine crystals of orthopyroxene and clinopyroxene in the andesites are consistent with the subsequent

differentiation (Fig. 4a,b). Extensive resorption and zoning textures in the plagioclase crystals (Fig. 3a-d) record mixing of several batches of magma, a process that is common in most arc volcanoes (Volpe, 1992; Bourdon et al, 2000; Davidson, et al., 1990, Cooper and Reid, 2003). Some of the crystals in the andesites (Fig. 3e,f) appear to be derived from disaggregated cumulate (Dungan and Davidson 2005), also consistent with mixing and entrainment of crystals during magma ascent. Together with the stratigraphic variation, it appears that the magma reservoir at Cotopaxi volcano was recharged at least 16 times since 13,200 years ago (Fig. 12a, b). Increases in MgO and Sr contents of the erupted lavas indicate that the composition of the recharge magma is variable, and the system has not become more evolved during the recent history of this volcano. There is no systematic general trend towards more (or less) evolved magmas through time among the andesites or the rhyolites, although the frequency of rhyolite eruptions is greater in the earlier eruptive phase studied in our work (Cotopaxi IIA).

The Cotopaxi rhyolites – small eruptions from a large reservoir?

The Cotopaxi rhyolites are somewhat enigmatic; even in continental arcs, repeated eruptions of rhyolite are uncommon at individual arc volcanoes. In most cases, rhyolite is associated with large caldera systems where long storage times allow for extensive fractionation over time periods of 10^4 - 10^5 years (i.e. Yellowstone, Reid et al., 1997; Toba, Vasquez and Reid, 2004; de Silva, 2008; Taupo, Charlier et al., 2003), and dacites are increasingly believed to represent crystal-rich mush zones (Bachman and Bergantz, 2004). Density and viscosity differences in the upper crust likely cause stalling of cooling magma (Thompson et al., 2001; Feeley and Dungan, 1996), and one way that rhyolite is believed

to form is by extraction of liquid from a reservoir of crystal mush (e.g. the “rhyolite nursery” of Streck and Grunder, 2007). In some systems, the crystal mush zone is reheated and mobilized by recharge (Fish Canyon dacite; Parat et al., 2005; Bachmann and Bergantz, 2003).

Unlike large caldera eruptions (10^2 - 10^3 km 3), the Cotopaxi rhyolites are small volume (0.1- 8 km 3), they were erupted in five events that are separated by as little as 2,000 years, and they are erupted intermittently between andesite events. The U-series data yield a magma storage time of 74 ka for these rhyolites (Garrison et al., 2006; Fig. 9a). In order to reconcile this long timescale with the high frequency of rhyolite eruptions, however, requires that the reservoir is long-lived, but tapped at repeated intervals of several thousand years. Extraction of small batches of magma that erupt periodically, perhaps triggered by recharge (Watts et al., 1999) or critical volume (0.1-8 km 3) and degassing, could explain the small-volume frequent eruptions and the aphyric texture of the rhyolite. We explain this by proposing that there is a long-lived mush zone, heated by fluxing andesite that contains a high-SiO₂ melt fraction that is periodically erupted. One problem with this model is the heat required to keep a large rhyolite reservoir thermally viable for 74,000 years, and producing only small increments of magma from the reservoir. If the rhyolite eruptions represent single batches of rhyolite liquid, then the U-series data require that there is a source with higher ($^{230}\text{Th}/^{232}\text{Th}$) that is melted or tapped to produce rhyolite eruptions. Remelting of old (>350 ka) andesites with high initial U-excesses could explain this, however it is difficult to explain the co-linear mineral-glass isochrons in the Cotopaxi rhyolites (Fig. 9b).

Numerical models of gas-driven filter pressing (compaction) (McKenzie, 1984; Shirley, 1986; Philpotts et al., 1996; Rabinowicz et al., 2001) and hindered settling (Bachman and Bergantz, 2004) were used to calculate how much time is required to physically separate the volumes of Cotopaxi rhyolite from a static crystal mush. We used estimated rhyolite volumes of $0.1 \text{ km}^3 - 8.4 \text{ km}^3$ (Hall and Mothes, 2008) and the parameters and equations detailed in Bergantz and Bachman (2004). A reservoir diameter of 7 km was used, on the basis of the diameter of the pre-existing Cotopaxi Caldera (Hall and Mothes, 2008). Melt-extraction models require that the interstitial glass in the crystal mush is rhyolitic, and that the crystals form an interlocking mesh (40-60% crystalline) (Bacon & Druitt, 1988; Sisson & Bacon, 1999; Hildreth & Fierstein, 2000). The Cotopaxi andesite glass compositions range from 60-78 wt % SiO_2 (Fig. 6). Figure 11b shows that the rhyolites could reasonably be derived from an andesite that is within the range of 40-50 % crystalline. To generate the $\sim 8 \text{ km}^3$ of the largest Cotopaxi rhyolite using hindered settling requires 2,000 years; compaction, on the other hand requires 45,000 years to produce the same volume of magma. These models show that in order to generate the smallest erupted volume (0.1 km^3) using the hindered settling model requires ~ 300 years, 2000 years using compaction. On the basis of these models, timescales of rhyolite formation (10^5 years for 8.4 km^3) are roughly consistent with the U-series estimates of 74,000 years; the small volume eruption estimates are consistent with the 2,000 repose interval of the Cotopaxi rhyolites. If the Cotopaxi U-series data represent a protracted crustal storage time (~ 74 kyr), then small melt fractions removed from the crystal mush must represent aliquots removed as the entire system ages. Alternatively, if the rhyolites represent small batches of magma, formed over ~ 300 -2000 years, then each

batch must represent melting or remobilizing of andesite mush that has aged for sufficient time (> 350 ka) that it is close to equilibrium and has higher ($^{230}\text{Th}/^{232}\text{Th}$) than the andesites. Once melted, the rhyolite is extracted from the mush, and accessory mineral fractionation (apatite, alanite, monzanite) creates the observed ^{238}U excesses (Fig. 9d). The rhyolite mineral isochrones are not explained by this model, and require further analysis.

The geochemical evidence that supports rhyolite formation by melt extraction from andesite crystal mush includes the overlapping $^{87}\text{Sr}/^{86}\text{Sr}$ and $^{143}\text{Nd}/^{144}\text{Nd}$ isotope data for the rhyolites and andesites (Fig. 8). Also, the compositions of the plagioclase crystals from the rhyolitic magma (An₂₄₋₅₀; Fig. 5) do not overlap with the composition of the andesite plagioclase (An₅₀₋₈₀) which, in addition to the pristine texture of the rhyolite plagioclase, suggests that crystals formed in a more evolved magma reservoir. The clinopyroxene crystals in one of the rhyolites have the same composition as the andesite clinopyroxene (Fig. 5b), which infers that these crystals formed in an andesitic magma and were entrained during segregation of the rhyolite from the andesite matrix. Physical evidence of crustal assimilation in the Cotopaxi system is the Precambrian recycled zircon crystals that are found in the rhyolite (Fig. A3). It is impossible to know at what point the zircon were inherited by the magma, although the lack of correlation between $^{87}\text{Sr}/^{86}\text{Sr}$ and wt % SiO₂ (Fig. 13) suggests that is not related to rhyolite formation by melting of radiogenic upper crust, which would have imparted a higher $^{87}\text{Sr}/^{86}\text{Sr}$ signature to the rhyolite. We propose that the rhyolites formed by segregation of melt with 62-78 wt % SiO₂ (Fig. 6) from an andesite mush containing clinopyroxene, orthopyroxene and plagioclase. Crystallization of plagioclase (50 %) + amphibole (25%) + biotite (15%)

+quartz (8%) + accessory minerals (2 %), is consistent with the observed variation in the trace elements of the rhyolite glass (Fig. 14).

SUMMARY AND CONCLUSIONS

- 1) The petrogenetic processes that formed the Cotopaxi andesites include assimilation of lower crustal melts of radiogenic crust similar to the metapelitic schist of the Raspas Terrain (Fig. 15, box 1). Lower crustal melts (5-20 %) of metapelitic crust mix with primitive basalt, creating the range $^{143}\text{Nd}/^{144}\text{Nd}$, $^{87}\text{Sr}/^{86}\text{Sr}$ and $^{207}\text{Pb}/^{204}\text{Pb}$ variation that is observed in the Cotopaxi rocks. This is also consistent with the oxygen isotope data of the Cotopaxi rocks and previously published U-series data (Garrison et al., 2006).
- 2) Minerals from the Cotopaxi rhyolites and andesites record a rich petrogenetic history, including early crystallization of olivine, followed by fractionation of clinopyroxene + orthopyroxene + plagioclase. Amphibole, although not a stable phase during eruption, is an important phase in the early stages of magmagenesis; the observed trace element variation cannot be reproduced in the absence of hornblende crystallization. Extensive mixing is recorded by at least four populations of plagioclase crystals, and the stratigraphy records at least 16 recharge events in the past 13,200 years (Fig. 15, box 2).
- 3) The Cotopaxi rhyolites are formed in the upper crust by compaction of andesite crystal mush and extraction of rhyolite liquid 74,000 years ago, followed by crystallization of plagioclase, amphibole and biotite (Fig 15, box 3]. Small batches of rhyolite magma are periodically erupted from a large magma reservoir, perhaps triggered by reheating of andesite magma. Alternatively, the individual rhyolite eruptions represent remelting of

andesite that had ^{238}U excesses and are older than 350 ka. Zircon crystals in the rhyolites record assimilation of the 2.1 crust of the South American craton.

4) The configuration of the rhyolite-andesite plumbing at Cotopaxi is not clear from this study. What controls the eruption of the rhyolite batches, particularly in the midst of repeated andesite eruptions? How does this relate to the timescales suggested by the existing U-series data? What is the relationship between the Colorado Canyon rhyolite and the Chalupas Caldera rhyolite? These questions remain to be answered, particularly regarding the short repose time and small volumes of the rhyolite eruptions and the trigger for andesite versus rhyolite eruptions. The data from Cotopaxi Volcano records a rich history of assimilation, magma mixing and crystallization processes in the Northern Volcanic Zone of South America. Combining stratigraphy with geochemistry adds a valuable component to studies of arc volcanoes and the evolution of continental arcs over time. These data reveal the many intricate processes involved in the sub-volcanic plumbing system of arc volcanoes and ultimately in the formation of continental crust.

ACKNOWLEDGEMENTS

This paper was greatly benefitted by thoughtful and thorough reviews by Gene Yogodzinsky, Dennis Geist and an anonymous reviewer. We also thank Mary Reid, Frank Ramos, Frank Tepley, John Hora and fellow students and staff at UCLA for helpful discussions during the development of this project. We are grateful to NSF for providing funding for this research. We also thank Dave Mattey and Dave Lowry at Royal Holloway, University of London for their help with oxygen isotope analyses, and the

students (Indira Molina and Alex Garcia) at the IGEPN in Quito, Ecuador for their help with field support.

REFERENCES

- Arculus, R. J., Lapierre, H. & Jaillard, E. (1999). Geochemical window into subduction and accretion processes: Raspas Metamorphic Complex, Ecuador. *Geology* **27**, 547-550.
- Alonso-Perez, R., Muñtener, O. & Ulmer, P. (2009). Igneous garnet and amphibole fractionation in the roots of island arcs: experimental constraints on andesitic liquids. *Contributions to Mineralogy and Petrology* **157**, 541-558.
- Bachmann, O. & Bergantz, G.W. (2004). On the Origin of Crystal-poor Rhyolites: Extracted from Batholithic Crystal Mushes. *Journal of Petrology* **45**, 1565-1582.
- Bachmann, O. & Bergantz, G.W. (2003). Rejuvenation of the Fish Canyon magma body: a window into the evolution of large-volume silicic magma systems. *Geology* **31**, 789-792.
- Bacon, C.R. & Druitt, T.H. (1988). Compositional Evolution of the Zoned Calcalkaline Magma Chamber of Mount-Mazama, Crater Lake, Oregon. *Contributions to Mineralogy and Petrology* **98**, 224-256.
- Baker, M.B, Grove, T.L. & Price, R. (1994). Primitive basalts and andesites from the Mt. Shasta region, N. California: products of varying melt fraction and water content. *Contributions to Mineralogy and Petrology* **118**.
- Barberi, F., Coltelli, M., Frullani, A., Rosi, M., & Almeida, E. (1995). Chronology and dispersal characteristics of recently (last 5000 years) erupted tephra of Cotopaxi (Ecuador): implications for long term eruptive forecasting. *Journal of Volcanology and Geothermal Research* **69**, 217-239.
- Barragan, R., Geist, D., Hall, M., Larson, P., & Kurz, M. (1998). Subduction controls on the compositions of lavas from the Ecuadorian Andes. *Earth and Planetary Science Letters* **154**, 153–166.
- Bigazzi G., Coltelli M., Hadler, J., & Osorio, A. (1997). Provenance studies of obsidian artifacts using fission track analyses in South America: An overview. *Mem 49th Cong Intern Americanistas, Quito, ARQ* **14**, 1-16.
- Bosch, D., Gabriele, P., Lapierre, H., Malfere, J.-L. & Jaillard, E. (2002). Geodynamic significance of the Raspas Metamorphic Complex (SW Ecuador): geochemical and isotopic constraints. *Tectonophysics* **345**, 83-102.
- Bottinga, Y. & Javoy, M. (2000). Oxygen isotope partitioning among the minerals in igneous and metamorphic rocks. *Reviews of Geophysics and Space Physics*. **13**, 401-418.

- Bourdon, B., Worner, G. & Zindler, A. (2000). U-series evidence for crustal involvement and magma residence times in the petrogenesis of Parinacota volcano, Chile. *Contributions to Mineralogy and Petrology* **139**, 458-469.
- Brenan, J.M., Shaw, H.F., Ryerson, F.J. & Phinney, D.L. (1995). Experimental-Determination of Trace-Element Partitioning between Pargasite and a Synthetic Hydrous Andesitic Melt. *Earth and Planetary Science Letters* **135**, 1-11.
- Bryant, J. A., Yogodzinski, G. M., Hall, M. L., Lewicki, J. L. & Bailey, D. G. (2006). Geochemical Constraints on the Origin of Volcanic Rocks from the Andean Northern Volcanic Zone, Ecuador. *Journal of Petrology* **47**, 1147–1175.
- Chadwick, J. P.; Troll, V. R.; Schulz, B.; Dallai, L.; Freda, C.; Schwarzkopf, L. M.; Annersten, H.; Skogby, H. (2010) The role of amphibole in Merapi arc magma petrogenesis: insights from petrology and geochemistry of lava hosted xenoliths and xenocrysts, *EGU General Assembly*, p. 15379.
- Charlier, B L.A., Peate, D W., Wilson, C J.N., Lowenstern, J B., Storey, M, & Brown, S, J.A. (2003). Crystallization ages in coeval silicic magma bodies: ^{238}U - ^{230}Th disequilibrium evidence from the Rotoiti and Earthquake Flat eruption deposits, Taupo Volcanic Zone, New Zealand. *Earth and Planetary Science Letters* **206**, 441-457.
- Chiaradia, M. (2009). Adakite-like magmas from fractional crystallization and melting-assimilation of mafic lower crust (Eocene Macuchi arc, Western Cordillera, Ecuador). *Chemical Geology* **265**, 468-487.
- Chiba H., Chacko T., Clayton R. N., & Goldsmith J. R. (1989). Oxygen isotope fractionations involving diopside, forsterite, magnetite and calcite: Application to thermometry. *Geochimica et Cosmochimica Acta* **53**, 2985-2995.
- Collot, J.Y., Calahorrano, A., Sage, F., Ranero, C., & P. Charvis. (2004a). Seismic reflection evidence for subduction erosion at the Ecuador trench, *Geophysical Research Abstracts* **6**, European Geosciences Union.
- Cooper, K. M., Reid, M.R. (2003). Re-examination of crystal ages in recent Mount St. Helens lavas: implications for magma reservoir processes, *Earth and Planetary Science Letters* **213**, 149-167.
- Dalrymple, B. G., Grove, M., Lovera, O. M., Harrison, T. M., Hulen, J B., Lanphere, M. A. (1999). Age and thermal history of the Geysers plutonic complex (felsite unit), Geysers geothermal field, California: a ^{40}Ar / ^{39}Ar and U-Pb study. *Earth and Planetary Science Letters* **173**, 285-298.
- Danyushevsky, L.V. (2001) The effect of small amounts of H_2O on crystallization of mid-ocean ridge and backarc basin magmas **100**, 265-280.

- Davidson, J.P., Turner, S.P., Handley, H., Macpherson, C. & A. Dosseto. (2007). Amphibole "sponge" in arc crust? *Geology* **35**, 787-790.
- Davidson, J. P. (1996). Deciphering mantle and crustal signatures in subduction zone magmatism. in *Subduction, top to Bottom*, Bebout, gray, E., Scholl, David W., Kirby, Stephen H., & Platt, John P., eds., *Geophysical Monograph* **96**, 251-261.
- Davidson, J.P., Harmon, R.S., & Worner, G. (1991). The source of central Andean magmas; some considerations. *Geological Society of America Special Paper* **265**, 233-243.
- Davidson, J.P., McMillan, N.J., Moorbath, S., Worner, G. Harmon, R.S. & Lopez-Escobar, L. (1990). The Nevados de Payachata volcanic region (18°S, 69°W, N. Chile) II. Evidence for widespread crustal involvement in Andean magmatism. *Contributions to Mineralogy and Petrology* **105**, 412-432.
- de Silva, S. (2008) Arc magmatism, calderas, and supervolcanoes *Geology* **36**, 671-672.
- Dungan, M.A. and Davidson, J.P., (2004). Partial assimilative recycling of the mafic plutonic roots of arc volcanoes: An example from the Chilean Andes. *Geology*; **32** 773–776.
- Feeley T. C. & Dungan M. A. (1996). Compositional and dynamic controls on mafic-silicic magma interactions at continental arc volcanoes: evidence from Cordon El Guadal, Tatara-San Pablo Complex, Chile. *Journal of Petrology* **37**, 1547–1577.
- Feininger, T. (1980). Eclogite and related high-pressure regional metamorphic rocks from the Andes of Ecuador. *Journal of Petrology* **21**, 107-140.
- Feininger, T. & Seguin, M. K. (1983). Simple Bouguer gravity anomaly field and the inferred crustal structure of continental Ecuador. *Geology* **11**, 40-44.
- Garrison, J. M., Davidson, J. P., Reid, M., & Turner, S. P. (2006). Source versus differentiation controls on U-series disequilibria: Insights from Cotopaxi Volcano, Ecuador. *Earth and Planetary Science Letters* **4**, 548-565.
- Garrison, J. M. (2004) Timescales of petrogenetic processes at Cotopaxi volcano, Northern Volcanic Zone, Ecuador, Ph.D. Dissertation, UCLA, 417 p.
- Garrison, J. & Davidson, J. P. (2003). A dubious case for slab melting in the Northern Volcanic Zone of the South American Andes. *Geology* **71**, 151-154.
- Guiller, B., Chatelain, J.L., Jaillard, E., Poupinet, G. & Fels, J.F. (2001). Seismological evidence on the geometry of the orogenic system in central-northern Ecuador (South America). *Geophysical Research Letters* **28**, 3749-3752.

- Hall, M. L., Samaniego, P., Le Pennec, J. L. & Johnson, J. B. (2008). Ecuadorian Andes Volcanism: A review of Late Pliocene to Present Activity. *Journal of Volcanology and Geothermal Research* **176**, 1-6.
- Hall, M. & Mothes, P. (2008). The rhyolitic-andesitic eruptive history of Cotopaxi volcano, Ecuador. *Bulletin of Volcanology* **70**, 675-702.
- Hall, M.L., & Mothes, P. (1995). A Bimodal nature of the eruptive history of Cotopaxi Volcano, Ecuador, International Union of Geodesy and Geophysics, General Assembly, **.21**, 452.
- Hall, M & Hillebrandt, von C. (1988). Mapa de los peligrosas volcánicos potenciales asociados con el volcán Cotopaxi: 1) zona norte y 2) zona sur. Instituto Geofisico, Quito.
- Harmon, R S; Barreiro, B A; Moorbat, S; Hoefs, J; Francis, P W; Thorpe, R S; Deruelle, B; McHugh, J; Viglino, J A. (1984). Reginal O-, Sr-, and Pb-isotope relationships in late Cenozoic calc-alkaline lavas of the Andean Cordillera, *Journal of the Geological Society of London* **141**, 803-822.
- Hart, S. R. (1984). A large-scale isotope anomaly in the Southern Hemisphere mantle, *Nature* **309**, 753-757.
- Hawkesworth, C., George, R., Turner, S., & Zellmer, G. (2004). Time scales of magmatic processes. *Earth and Planetary Science Letters* **218**, 1-16.
- Hawkesworth, C.J., Blake, S., Evans, P., Hughes, R., Macdonald, R., Thomas, L.E., Turner, S.P. & Zellmer, G. (2000) Time scales of crystal fractionation in magma chambers – Integrating physical, isotopic and geochemical perspectives. *Journal of Petrology* **41**, 991-1006.
- Hawkesworth, C.J., Turner, S.P., McDermott, F., Peate, D.W., and & van Calsteren, P. (1997). U-Th Isotopes in Arc Magmas: Implications for Element Transfer from the Subducted Crust. *Science* **276**, 551-555.
- Hildreth W. & Moorbat S. (1988). Crustal contributions to arc magmatism in the Andes of central Chile. *Contributions to Mineralogy and Petrology* **98**, 455-489.
- Hora, J.M., Singer, B.S., Worner, G., Beard, B., Jicha, B.R., Johnson C.M. (2009) Shallow and deep crustal control on differentiation of calc-alkaline and tholeiitic magma. *of Earth and Planetary Science Letters* **285**, 75-86
- Hughes, R. A., & Pilatasig, Luis F. (2002). Cretaceous and Tertiary terrain accretion in the Cordillera Occidental of the Andes of Ecuador. *Tectonophysics* **345**, 29-48.

- James, D. E., Murcia, A.L. (1984). Crustal contamination in northern Andean volcanics. *Journal of the Geological Society of London* **141**, 823-830.
- Johnson, D.M., Hooper P.R., and Conrey, R.M.,(1999) XRF Analysis of Rocks and Minerals for Major and Trace Elements on a Single Low Dilution Li-tetraborate Fused Bead *Advances in X-ray Analysis* **41**, 843-867.
- Knaak, C., Cornelius, S.B., Hooper, P.R. (1994). Technical notes: Trace Element Analyses of Rocks and Minerals by ICP-MS. *GeoAnalytical Lab, Washington State University*.
- Larocque, J. and Cani, D. (2009). The role of amphibole in the evolution of arc magmas and crust: the case from the Jurassic Bonanza arc section, Vancouver Island, Canada. *Contributions to Mineralogy and Petrology* **159**, 475–492.
- Le Maitre, R. W., Bateman, P., Dudek, A., Keller, Lameyre Le Bas, M.J., Sabine, P.A., Schmid, R., Sorenson, H., Streckeisen, A., Wooley, A.R., Zanettin, B. (1989). A classification of igneous rocks and a glossary of terms, Blackwell, Oxford. 342p.
- Lonsdale, P. (1978). Ecuadorian subduction system. *The American Association of Petroleum Geologists Bulletin* **62**, 2454-2477.
- Mamberti, M., Lapierre, Henriette, Bosche, Delphine, Jaillard, Etienne, Ethiene, Raynald, Hernandez, Jean & Polve Mireille. (2003). Accreted fragments of the Late Cretaceous Caribbean-Colombian Plateau in Ecuador. *Lithos* **66**, 173-199.
- McCourt, W. J., Aspden, J. A. & Brook, M. (1984). New geological and geochronological data from the Colombian Andes: continental growth by multiple accretion. *Journal of the Geological Society of London* **141**, 831-845.
- McDonough, W.F. and Sun, S.-S. (1995). Composition of the Earth. *Chemical Geology* **120**, 223-253.
- McKenzie, D. (1984). The generation and compaction of partially molten rock. *Journal of Petrology* **25**, 713-765.
- Mothes, P. (1992). Lahars of Cotopaxi volcano, Ecuador: hazard and risk evaluation. In *McCall GJH, Laming DJC, Scott SC (eds.)*, *Geohazards, natural and man-made*, 53-64.
- Mothes, P. & Hall, M., Andrade, D, Samaniego, P, Pierson, T, Ruiz, G, Yepes, H. (2004). Character, stratigraphy and magnitude of historical lahars of Cotopaxi volcano, Ecuador. *Acta Volcanology* **16**, 85-107
- Mothes, P., Hall, M, Janda, R. (1998). The enormous Chillos valley lahar: an ash-flow generated debris flow from Cotopaxi volcano, Ecuador. *Bulletin of Volcanology* **59**, 233-244.

- Parat, F., Dungan, M. A. & Lipman, P. W. (2005). Contemporaneous Trachyandesitic and Calc-alkaline Volcanism of the Huerto Andesite, San Juan Volcanic Field, Colorado, USA. *Journal of Petrology* **46**, 859-891.
- Peacock, S. M., (1990) Fluid processes in subduction zones, *Science* **248**, 329–337.
- Philpotts, A. R., Carroll, M. & Hill, J. M. (1996). Crystal-mush compaction and the origin of pegmatitic segregation sheets in a thick flood-basalt flow in the Mesozoic Hartford Basin, Connecticut. *Journal of Petrology* **37**, 811-836.
- Plank, T. and Langmuir, C. H., (1998) The chemical composition of subducting sediment and its consequences for the crust and mantle, *Chemical Geology* **145**, 325–394
- Rabinowicz, M., Genton, P., Ceuleneer, G. & Hillairet, M. (2001). Compaction in a mantle mush with high melt concentrations and the generation of magma chambers. *Earth and Planetary Science Letters* **188**, 313-328.
- Reid, M. R., Coath, C.D., Harrison, M.T., & McKeegan, K.D. (1997). Prolonged residence times for the youngest rhyolites associated with Long Valley Caldera: ^{230}Th - ^{238}U ion microprobe dating of young zircons. *Earth and Planetary Science Letters* **150**, 27-39.
- Ribeiro-Lauret., M. (2008). Adakitic Magmas: Amphibole Composition and Geobarometric Constraints. *Geological Society of America Abstracts with Programs* **40**, 249.
- Schmidt, M. W., Dardon, A., Vannucci, R. & Chazot, R. (2004). The dependence of Nb and Ta rutile-melt partitioning on melt composition and Nb/Ta fractionation during subduction processes. *Earth and Planetary Science Letters* **226**, 415-432.
- Shaw, S.D., DeBari, S., Wallace, P. and Sisson, T., 2010, Volatile contents in olivine-hosted melt inclusions from primitive magmas in the Northern Cascade arc: 2010 AGU Fall Meeting, V53C-2260
- Shirley, D. N. (1986). Compaction in igneous cumulates. *Journal of Geology* **94**, 795-809.
- Sisson, T. W. & Bacon, C. R. (1999). Gas-driven filter pressing in magmas. *Geology* **27**, 613-616.
- Streck, M. J., Grunder, Anita (2007). Phenocryst-poor rhyolites of bimodal, tholeiitic provinces: the Rattlesnake Tuff and implications for mush extraction models. *Bulletin of Volcanology* **70**, 385-401.
- Sun, S. S. & McDonough. (1989). Chemical and isotopic systematics of oceanarc basalts: implications for mantle composition and processes. *Geological Society of London Special Publication* **42**, 313-345.

- Spikings, R. A., Winkler, T., W., Hughes, R. A. & 2005, H. R. (2005). Thermochronology of allochthonous terranes in Ecuador: Unravelling the accretionary and post-accretionary history of the Northern Andes, *Tectonophysics* **399**, 195-220.
- Taboada, A., et al. (2000), Geodynamics of the northern Andes: Subductions and intracontinental deformation (Colombia), *Tectonics* **19**, 787-813.
- Tamura, Y., Yuhara, M. and Ishi, T. (2000) Primary Arc Basalts from Daisen Volcano, Japan: Equilibrium Crystal Fractionation versus Disequilibrium Fractionation during Supercooling, *Journal of Petrology* **41**, 431–448.
- Tera, F. & Wasserburg, G. J. (1974). U-Th-Pb systematics on lunar rocks and inferences about lunar evolution and the age of the moon. Proceedings from the 5th Lunar Science Conference (Supplement 5). *Geochimica et Cosmochimica Acta* **2**, 1571-1599.
- Thompson, G., Malpas & Smith, I. (2001). Origin of oceanic phonolites by crystal fractionation and the problem of the Daly gap: An example from Rarotonga. *Contributions to Mineralogy and Petrology* **142**, 336-346.
- Tiepolo, M., Bottazzi, P., Foley, S.F., Oberti, R., Vannucci, R., Zanetti, A., (2000) Fractionation of Nb and Ta from Zr and Hf at mantle depths: the role of titanian pargasite and kaersutite. *Journal of Petrology* **42**, 221-232.
- Turner, S. P., George, R. M., Evans, P. J., Hawkesworth, C. J. & Zellmer, G. F. (2000). Timescales of magma formation, ascent and storage beneath subduction-zone volcanoes. *Philosophical Transactions of the Royal Society of London* **358**, 1443-1464.
- Vazquez, J. A., Reid, M. R (2004). Probing the Accumulation History of the Voluminous Toba Magma. *Science* **305**, 991.
- Volpe, A. M. (1992). ^{238}U - ^{230}Th - ^{226}Ra disequilibrium in young Mt. Shasta andesites and dacites. *Journal of Volcanology and Geothermal Research* **53**, 227-238.
- Watts, R B; de Silva, S L; Jimenez de Rios, G; Croudace, I, (1999) Effusive eruption of viscous silicic magma triggered and driven by recharge; a case study of the Cerro Chascon-Runto Jarita Dome Complex in Southwest Bolivia, *Bulletin of Volcanology*, **61**, 241-264.
- White, W. M., McBirney, A. R. & Duncan, R. A. (1993). Petrology and geochemistry of the Galapagos islands: portrait of a pathological mantle plume. *Journal of Geophysical Research* **98**, 19533–19563.

Wolff, J. A., Balsley, S. D. & Gregory, R. T. (2002). Oxygen isotope disequilibrium between quartz and sanidine from the Bandelier Tuff, New Mexico, consistent with a short residence time of phenocrysts in rhyolitic magma. *Journal of Volcanology and Geothermal Research* **116**, 119-135.

Wolf, T. (1878). Memoria sobre el Cotopaxi y su última erupción acaecida el 26 de junio de 1877. *Imprenta, El Comercio, Guayaquil*, 4

FIGURE CAPTIONS

Figure 1. A) Location map of the Northern Volcanic Zone (NVZ) in Ecuador, South America. The Central, Southern and Austral volcanic zones (CVZ, SVZ, AVZ, respectively) are shown for comparison. RMC; Approximate location of the Raspas Metamorphic Complex, from Arculus et al. (1999) and Bosch et al. (2002). B) Expanded region from 1A showing Ecuador and the locations of Cotopaxi and Chalupas Caldera, C) DEM image showing the location of the volcanoes nearest to Cotopaxi, including volcanoes Pasachoa, Ruminaui, Sincholagua and the approximate outline of the Chalupas Caldera. The Morurcu satellite vent located on the south flank of Cotopaxi Volcano.

Figure 2. A) Generalized stratigraphic column of Cotopaxi deposits (Hall and Mothes, 2008). Gray and white regions represent generalized andesite and rhyolite sequences. B) Wt % K₂O vs. SiO₂ showing rock name classification of LeMaitre (1989) and C) wt % MgO vs. SiO₂ for the Cotopaxi IIA & IIB series, showing the compositional range of the Cotopaxi IIA and IIB sequences. The dashed lines separate the fields for basaltic andesite, andesite, dacite and rhyolite. The shaded region represents the range of Chalupas Caldera values.

Figure 3. Photomicrographs of plagioclase populations from Cotopaxi andesite and rhyolite, showing A) plagioclase with resorbed cores, B) resorbed rims, C) near entire resorption of plagioclase, D) pristine crystals, E) plagioclase crystals with melt inclusions and F) an equilibrium intergrowth of plagioclase (pl), orthopyroxene (opx) and clinopyroxene (cpx) in one of the andesites. Scale bars are shown on all photos.

Figure 4. Photomicrographs showing A) a pristine orthopyroxene crystal in the Cotopaxi andesite, B) a pristine clinopyroxene crystals with a Mg-rich core, C) orthopyroxene with olivine inclusions in a basaltic andesite D) a highly resorbed amphibole in the Morurcu andesite, E) pristine but broken plagioclase from the Cotopaxi rhyolite and F) a pristine amphibole crystal in one of the Cotopaxi rhyolites.

Figure 5. A) Anorthite content (An#) in plagioclase from Cotopaxi andesites (An₅₀₋₈₀) and rhyolites (An₂₄₋₅₂), showing slight overlap between the two compositions, as shown by the parallel dashed lines. B) Pyroxene quadrilateral, showing the compositional range of the rhyolite and andesite.

Figure 6. K₂O versus SiO₂ for several glass and whole-rock pairs from Cotopaxi andesites and rhyolites. The whole compositions are shown as shaded gray regions. Minerals were analyzed using the JEOL electron microprobe at UCLA. Data in appendix Table A1.

Figure 7. Primitive mantle-normalized incompatible trace element (ITE) diagrams for **A**) the Cotopaxi IIA series and **B**) Cotopaxi IIB series. The field for Cotopaxi rhyolite is shown for comparison (gray shaded). The Chalupas rhyolite is plotted for comparison to the Colorado Canyon rhyolite. Normalization factors from Sun and McDonough, (1989). **C)** REE diagram for the rhyolites and andesites.

Figure 8. **A)** $^{87}\text{Sr}/^{86}\text{Sr}$ and $^{143}\text{Nd}/^{144}\text{Nd}$ isotopic variation for South America and for the Cotopaxi andesites and rhyolites (inset). Fields for NVZ, AVZ and CVZ are from Bourdon et al., (2003). The gray shaded region is the field for accreted terrain data are from the Macuchi Island Arc (Chiardia et al., 2009) and Caribbean ocean plateau (Mamberti et al., 2003). GA: garnet amphibolite. Raspas Terrain data are from Bosch et al., (2002). Error bars are smaller than symbols. Dashed line represents mixing between MORB and the Raspas metapelite ($^{87}\text{Sr}/^{86}\text{Sr} = 0.722$, $^{143}\text{Nd}/^{144}\text{Nd} = 0.512$). Numbers represent proportion of crust in the mix. The Cotopaxi data are consistent with a 10-20 % contribution from Raspas metapelite. **B)** $^{206}\text{Pb}/^{204}\text{Pb}$ vs. $^{207}\text{Pb}/^{204}\text{Pb}$ graph for the Cotopaxi rocks, fields for NVZ, AVZ and CVZ and the accreted terrains are the same as for 8A. Cotopaxi data are shown in inset. The Northern Hemisphere Reference Line (NHRL) from (Hart, 1984). Dashed line represents mixing between MORB and Raspas metapelite. The Cotopaxi data are consistent with a 5-15 % contribution from Raspas metapelite.

Figure 9. **A)** U-series data for Cotopaxi volcano andesites and rhyolites (for full discussion see Garrison et al., 2006). The andesite data span a range in $(^{238}\text{U})/(^{230}\text{Th})$ of 0.96–1.07, whereas the rhyolites have ^{238}U excesses of 3–14 %. The linear array of rhyolite data points yields a U-Th age of 74,000 years, inferred to be the crystallization time of the rhyolite reservoir. **B)** Rhyolite mineral and glass separates and whole rocks for two of the Cotopaxi rocks. **C)** Generalized process diagram illustrating possible causes of U-series disequilibria, including ^{230}Th excesses through lower crustal melting, followed by ^{238}U excesses generated by accessory phase fractionation. **D)** Alternative model to explain U-series data. The grey shaded region represents hypothetical melts with ^{238}U excesses that cool and reach equilibrium, imparting a higher $(^{230}\text{Th}/^{232}\text{Th})$ than the younger andesites. Re-melting of the older andesites followed by fractionation of accessory minerals produces the rhyolites with ^{238}U excesses.

Figure 10. $^{87}\text{Sr}/^{86}\text{Sr}$ vs. $\delta^{18}\text{O}$ for the Cotopaxi whole rocks and glass, illustrating that the Cotopaxi data are consistent with a crustal assimilation, rather than a source contamination trend. Cotopaxi data from this study are shown in the inset box. Shaded field represents Chalupas Caldera samples. Fields for the Southern, Central and Northern Volcanic Zones are drawn for comparison (data from Harmon et al., 1984). Error bars are smaller than symbol sizes. The upper arrow (crustal contamination) was modeled using the same end members as were used in Fig. 8; the Raspas Terrain metapelite. The $\delta^{18}\text{O}$ value for this end member was estimated on the basis of other radiogenic metapelitic rocks. Numbers represent proportion of crust in the mix. The Cotopaxi data are consistent with a 10–20 % contamination of the Raspas metapelite, not the garnet amphibolite.

Figure 11. **A)** La/Dy versus La/Yb, showing numerical models of fractional crystallization. D values are from Bacon and Druitt (1988) and Sisson and Bacon (1992). The andesites require crystallization of 30 % amphibole + 14 % plagioclase + pyroxene and olivine; the rhyolites could hypothetically be produced by crystallization of 36 % plagioclase + 24 % amphibole, plus biotite, quartz and accessory phases. **B)** Sr (ppm) versus La/Yb, using the same crystallizing assemblage in A. The gray star represents the

composition of arc basalt (Mt. Shasta, Baker et al., 1994), the gray shaded region represents the range of mixtures of arc basalt with 7-15% partial melt of lower crust (black star). The melting model is illustrated by the black dashed line. The solid black line represents crystallization of the same mineral assemblage from 1A for the andesite. The Morurcu vent samples are shown for comparison, and show a trend opposite of that to the younger andesites. D values used for models (Table A3) were experimentally derived for amphibole at 1000°C and 1.5 GPa (Brennen et al., 1995).

Figure 12. Compositional and temporal variation in the Cotopaxi IIA and IIB sequences. Symbols are consistent with previous figures. **A)** Variation in wt % MgO over time for the Cotopaxi erupted rocks. **B)** Variation in Sr content. These figures illustrate that 1) the system is frequently recharged, 2) the composition of the recharge magma is variable and 3) the system does not overall become progressively more evolved over time. Ages correspond to the generalized Cotopaxi II stratigraphy of Fig. 2a, younger than 13,200 years.

Figure 13. $^{87}\text{Sr}/^{86}\text{Sr}$ versus wt % SiO₂ for the Cotopaxi rocks, illustrating that there is no correlation between differentiation and Sr isotope variation, as might be expected if differentiation was related to crustal contamination. Error is smaller than symbol size.

Figure 14. ITE diagram showing the CTX-67 rhyolite glass composition compared to the range of Cotopaxi rhyolites (grey shading). Depletions in Ti and the M REE are consistent with amphibole and rutile fractionation.

Figure 15. Schematic petrogenetic model used to explain the geochemical variation among the Cotopaxi andesites and rhyolites (modified from Garrison et al., 2006). Boxes described in text.

Appendix Figures

Figure A1. Shaded relief map of the Cotopaxi region, showing locations of samples used in this study. Image from Hall and Mothes, 2008.

Figure A2. Diagram showing modal abundance of crystals and glass versus wt % SiO₂ for pyroclastic deposits and lava flows A, B and D.

Figure A3. A) Illustrative diagram showing the general relationship between the ages of the seven Cotopaxi rhyolite zircon crystals and the zircon crystals from the Chalupas Caldera Ignimbrite. The width of each bar signifies the approximate age range. Actual ages were determined using Tera-Wasserburg diagrams (Tera and Wasserburg, 1974). **B)** Cathodoluminescence images of zircon crystals from the Chalupas Caldera Ignimbrite and one of the Cotopaxi rhyolites (CTX 19).

Figure A4. Oxygen isotope temperature data for a subset of the Cotopaxi samples. Temperatures are calculated using fractionation factors from Chiba (1989) and Zheng

(1993). Mag-amphibole and mag-biotite data for the rhyolites are from Bottinga and Javoy (2000). Eruption ages are listed to the right of the temperature data.

Table 1. XRF and ICP data for the Cotopaxi samples. Samples labeled *a* and *b* are leaching experiments used to test for alteration. Both samples *a* (leached) and *b* (non-leached) are shown for comparison for several samples. Major elements and Ni, Cr, V and Zr were measured by XRF, all other trace elements were measured using ICP following the methods established by the GeoAnalytical Lab in Pullman, WA.

Table 2. Sr, Nd and Pb isotope data. Expanded fields show only the Cotopaxi data. Error bars are smaller than symbol size. NVZ data are from Gutscher et al (2001). Composition of Continental Crust is from Bryant et al., (2006). Fields for mantle components are from Hart et al (1978). The standard NBS-987 was used for Sr analysis, La Jolla was used for Nd, and NBS 981 was used for Pb analysis. The Pb ratios are not double-spiked.

Table 3. Oxygen isotopes for two rhyolites and andesites, using laser fluorination at the University College of London. Gore Mountain Garnet (GMG) and San Carlos olivine (SC) were used as standards.

Table A1. Electron microprobe data of Cotopaxi samples, analyzed using the JEOL JXA-8200 electron microprobe at UCLA.

Table A2. XLFrac results of least squares modeling of major elements. Data for the end members and crystallizing phases were analyzed using the electron probe (data in Table A1)

Figure 1

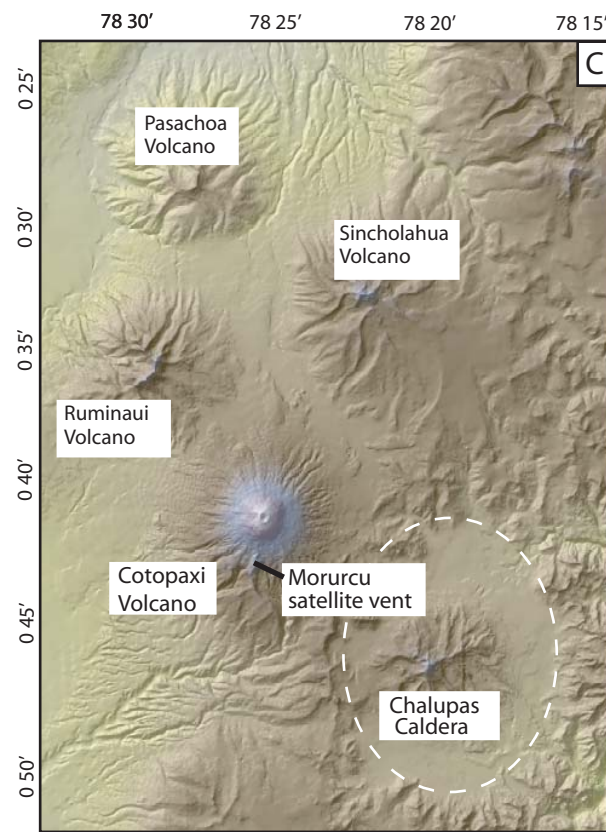
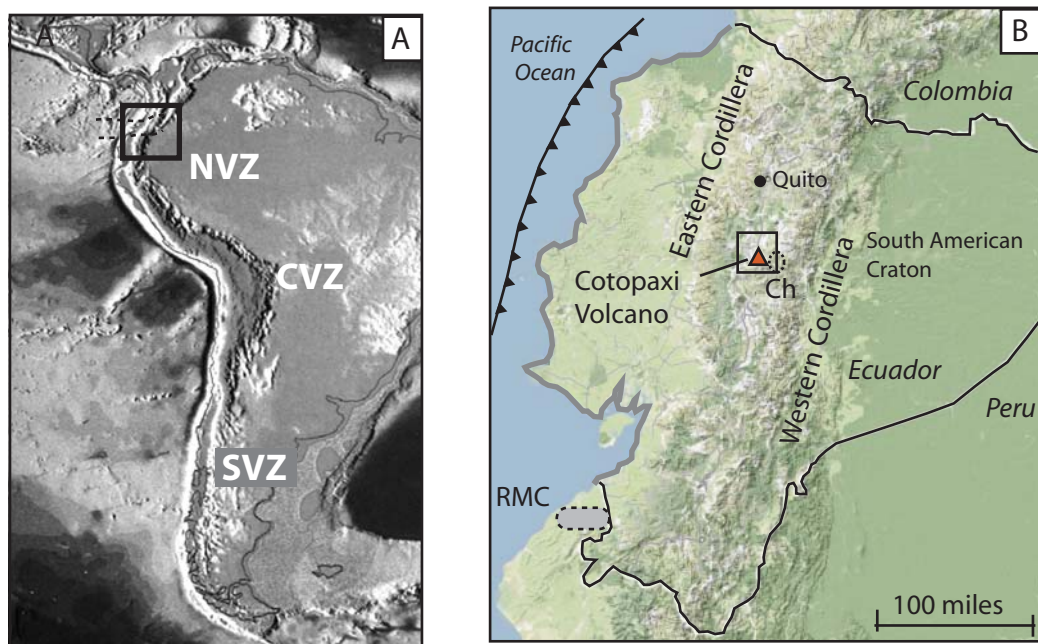


Figure 2

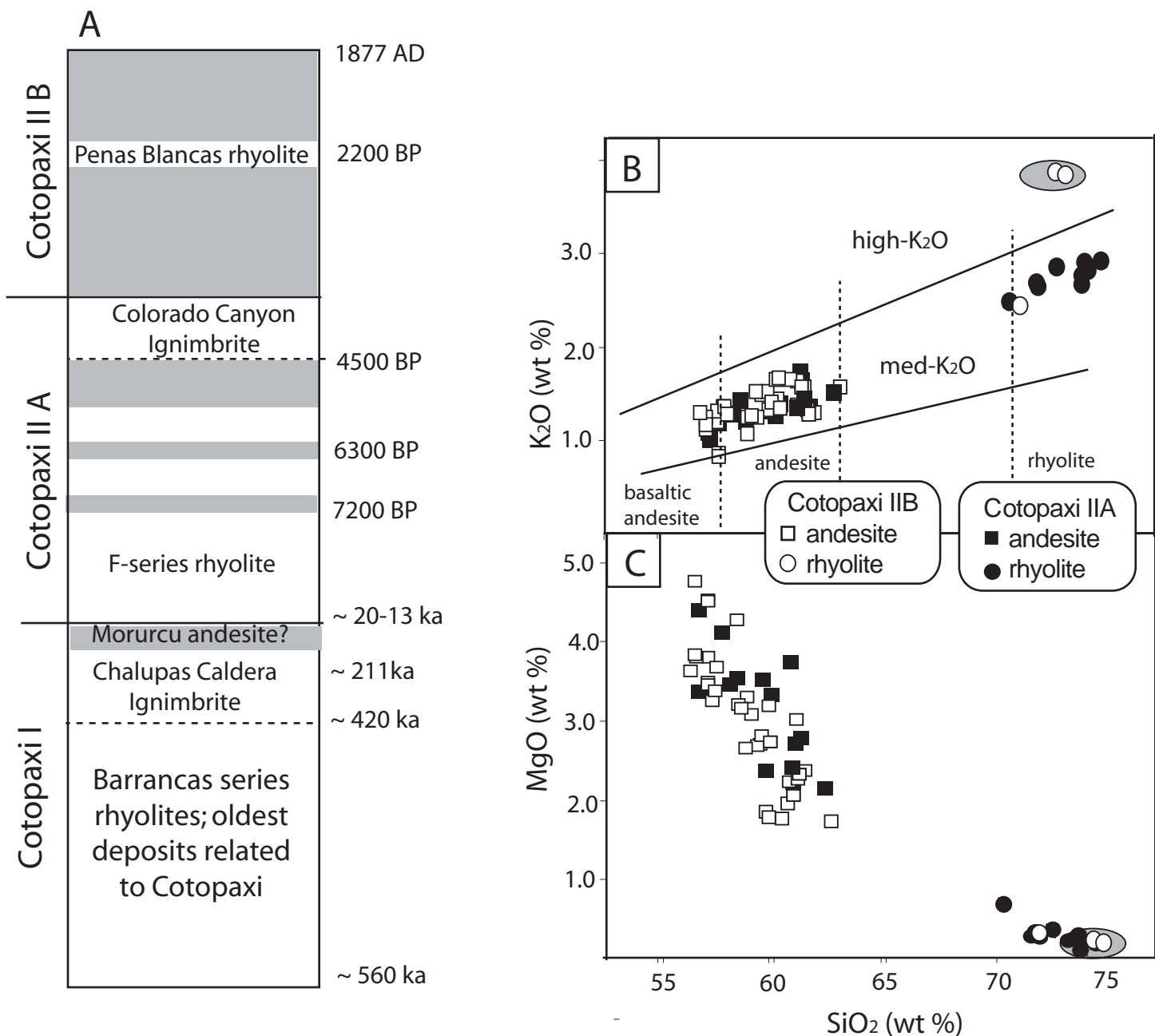


Figure 3

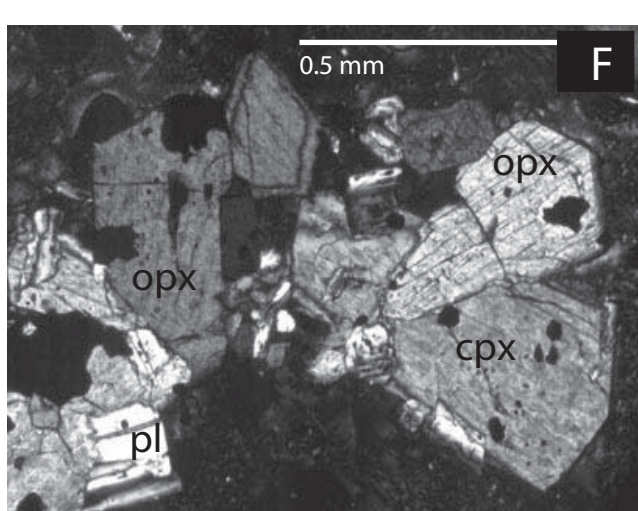
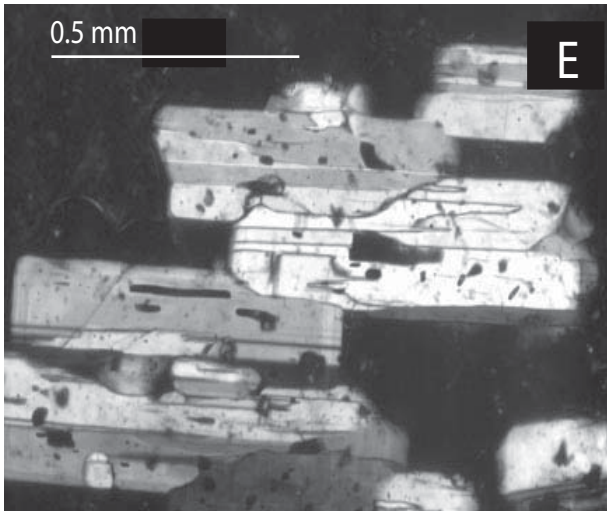
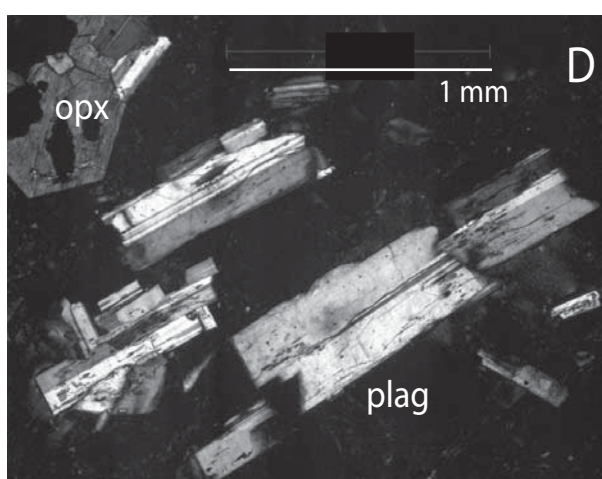
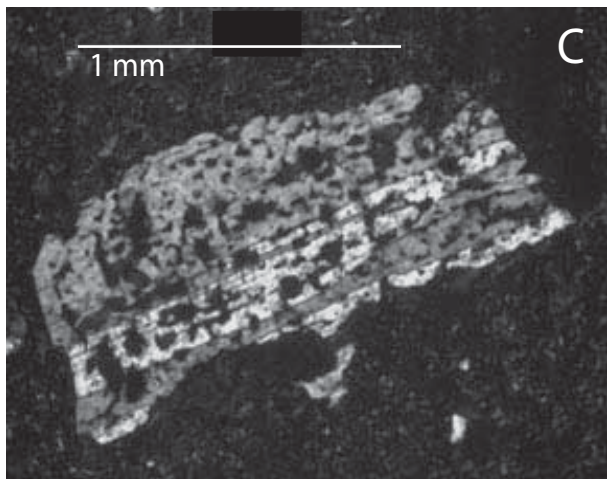
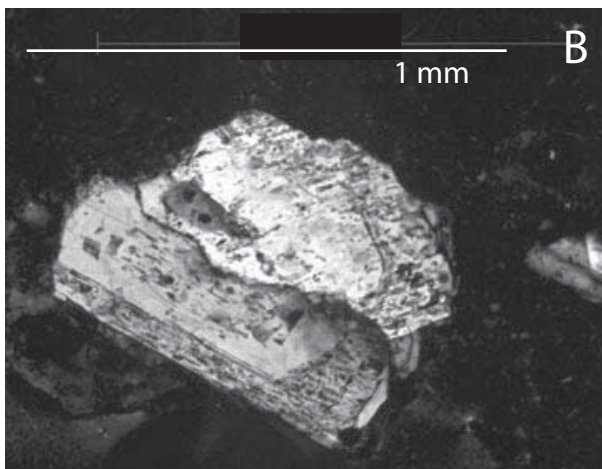
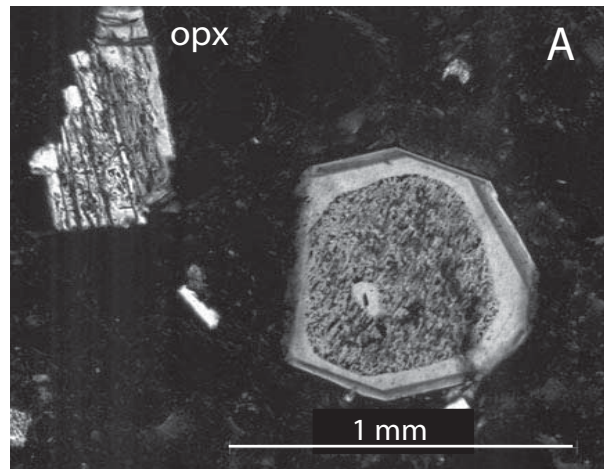


Figure 4

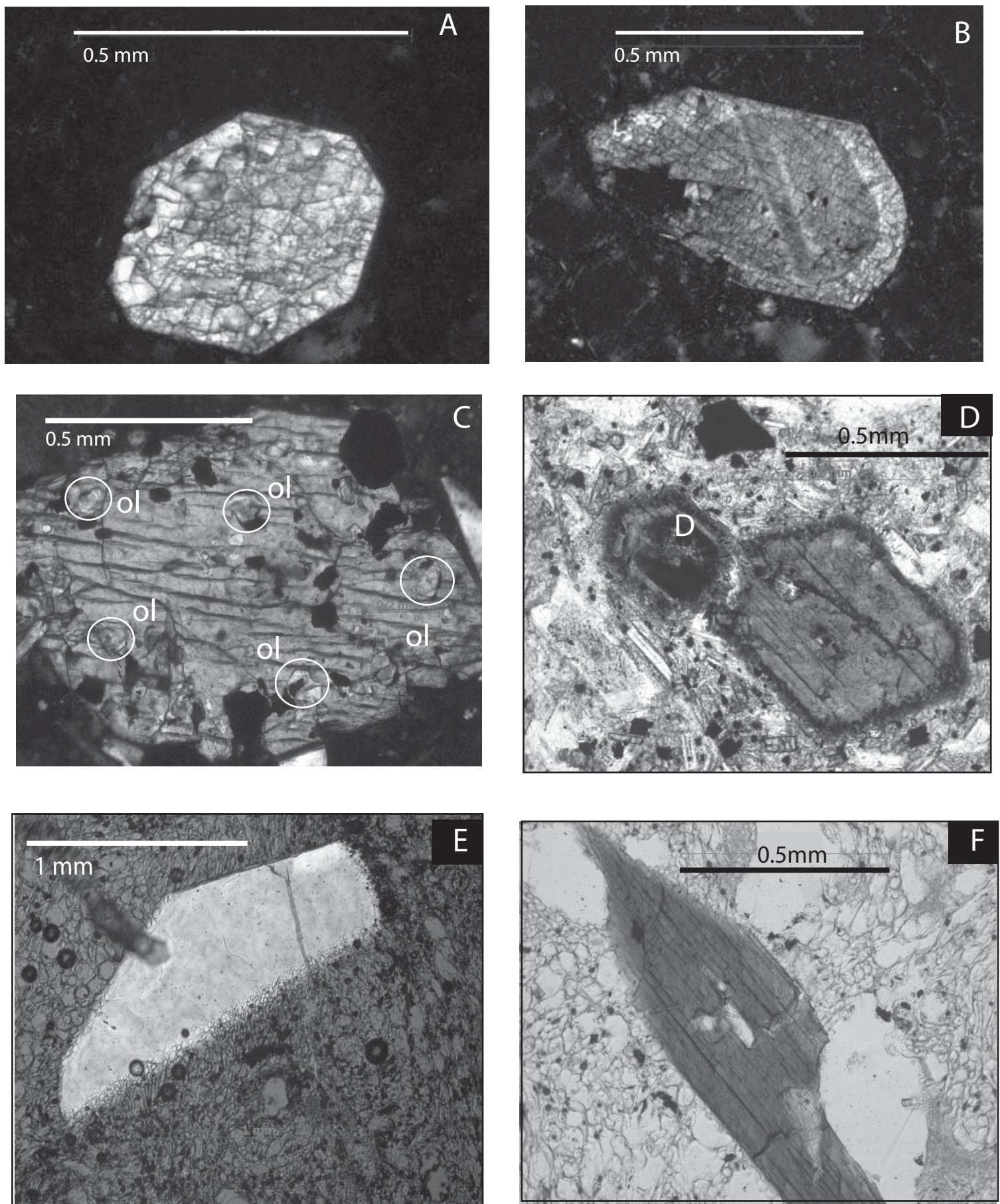


Figure 5

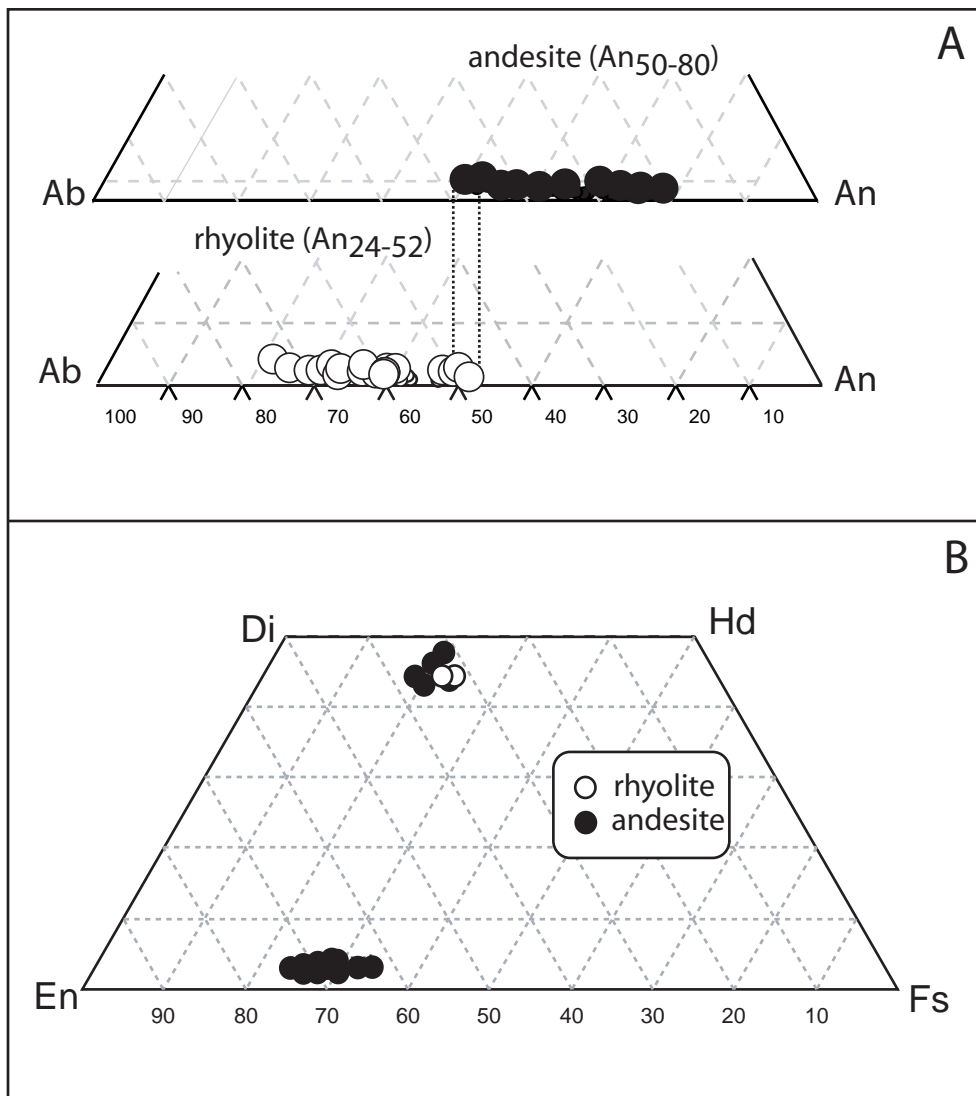


Figure 6

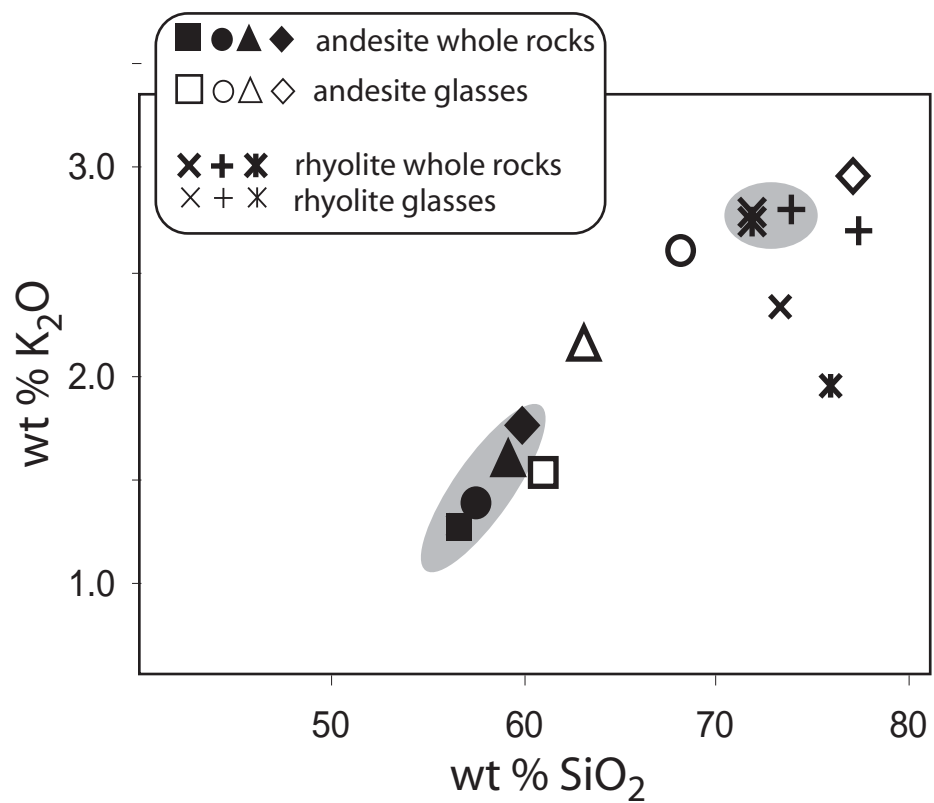


Figure 7

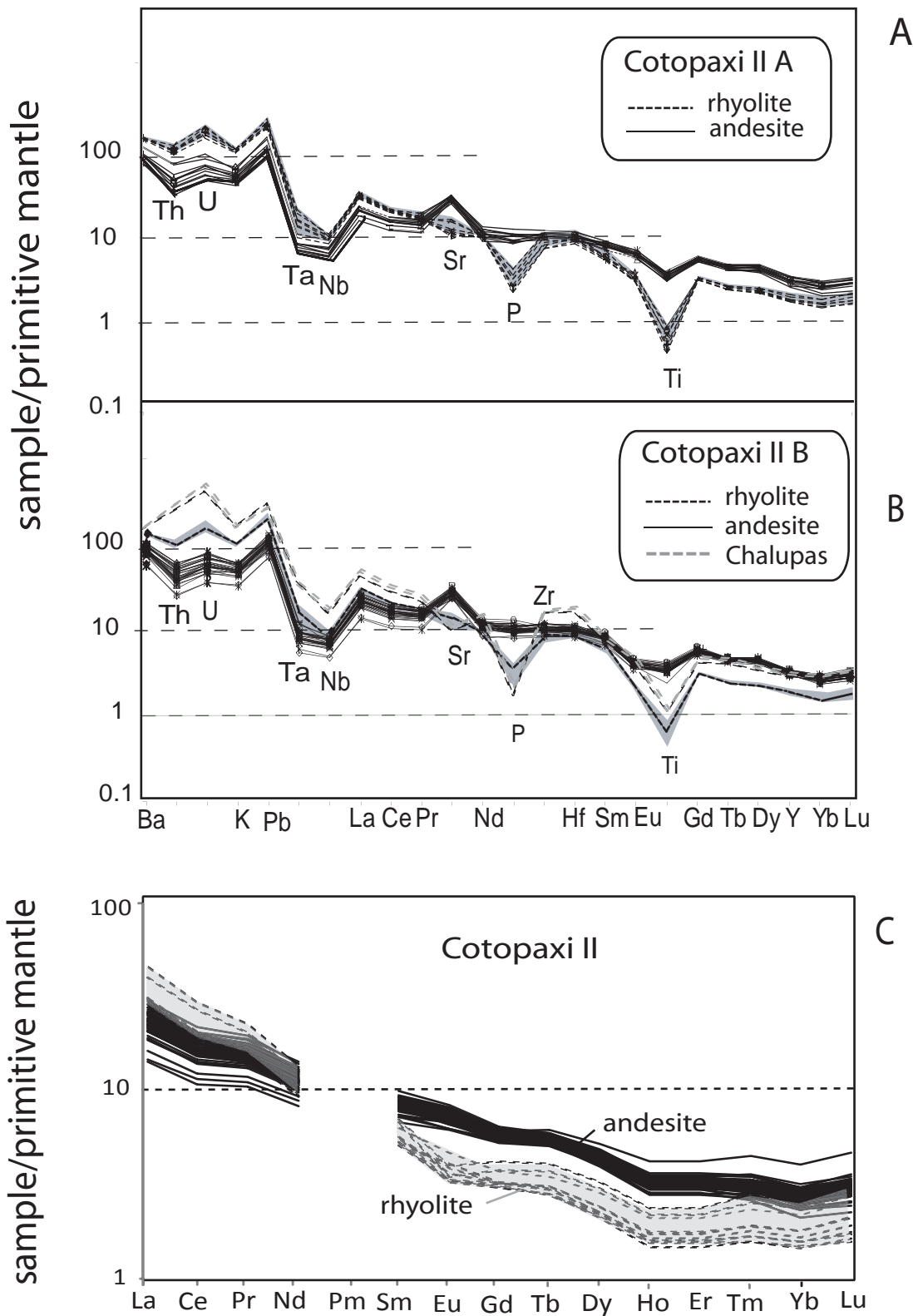


Figure 8

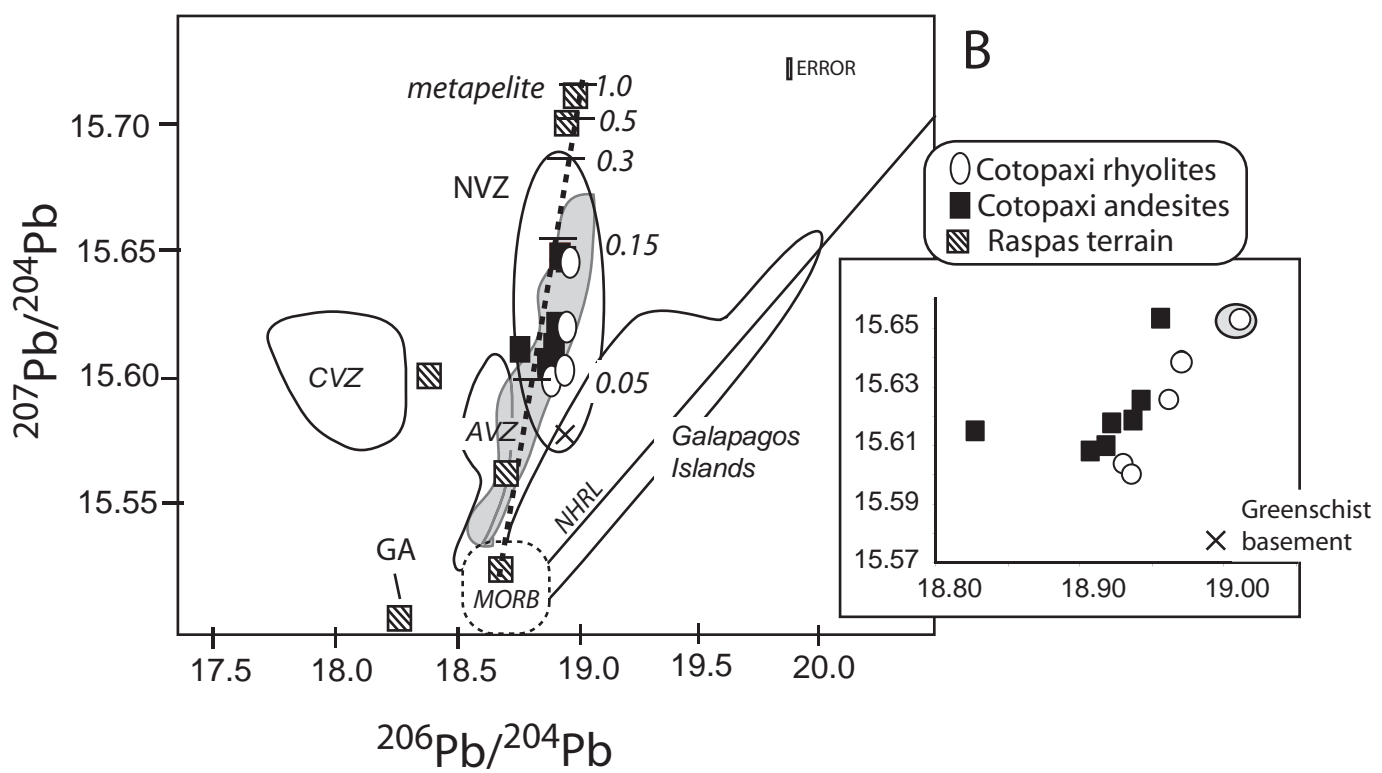
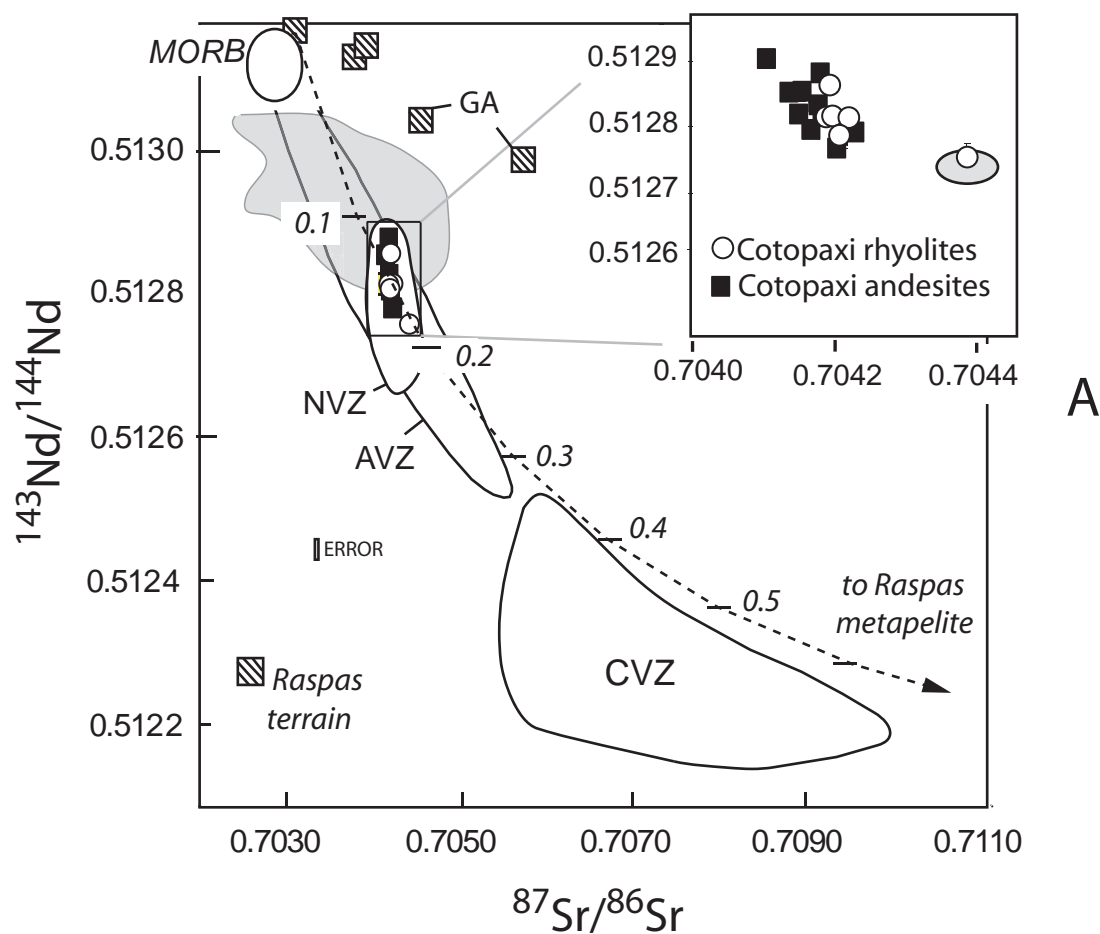


Figure 9

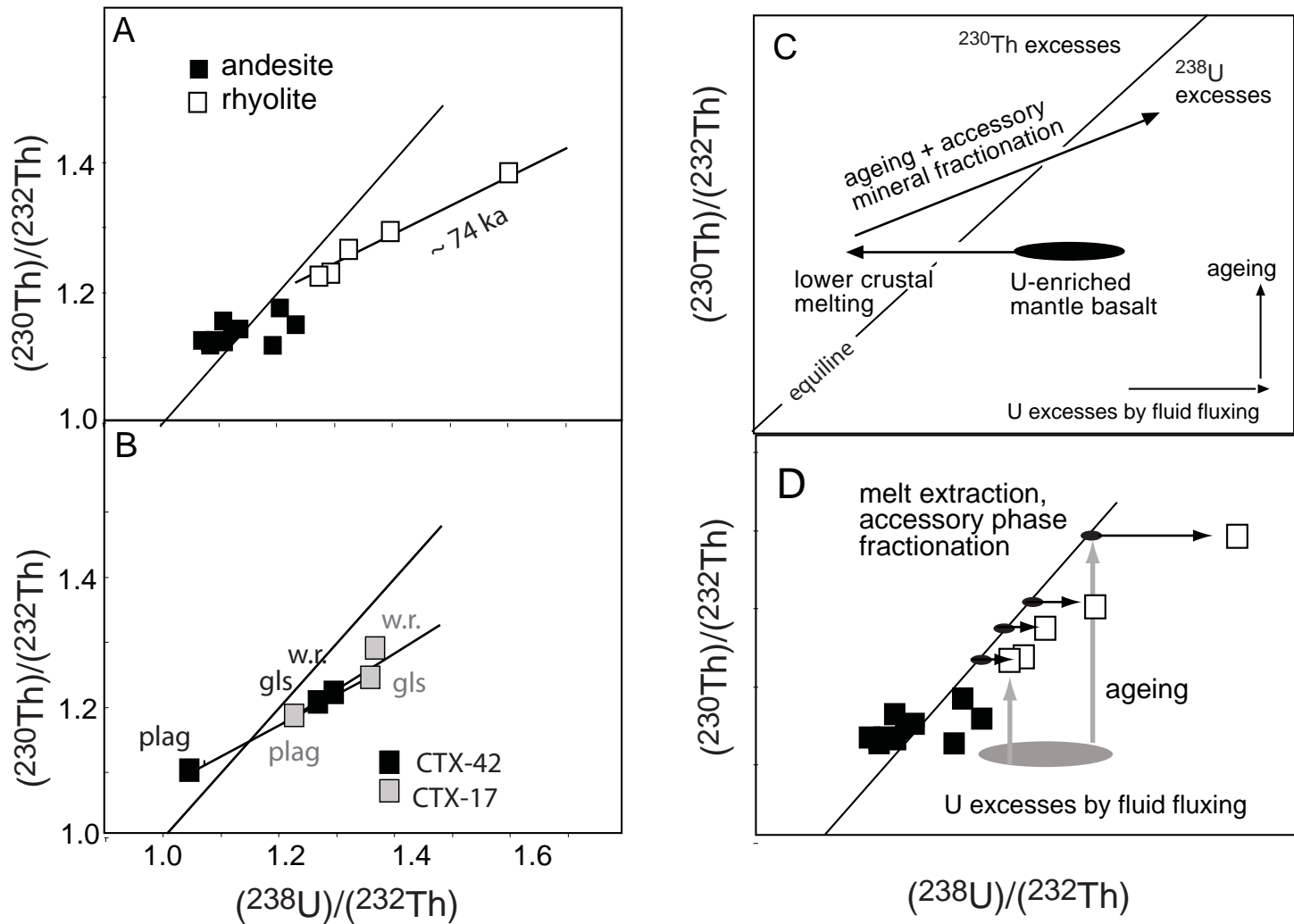


Figure 10

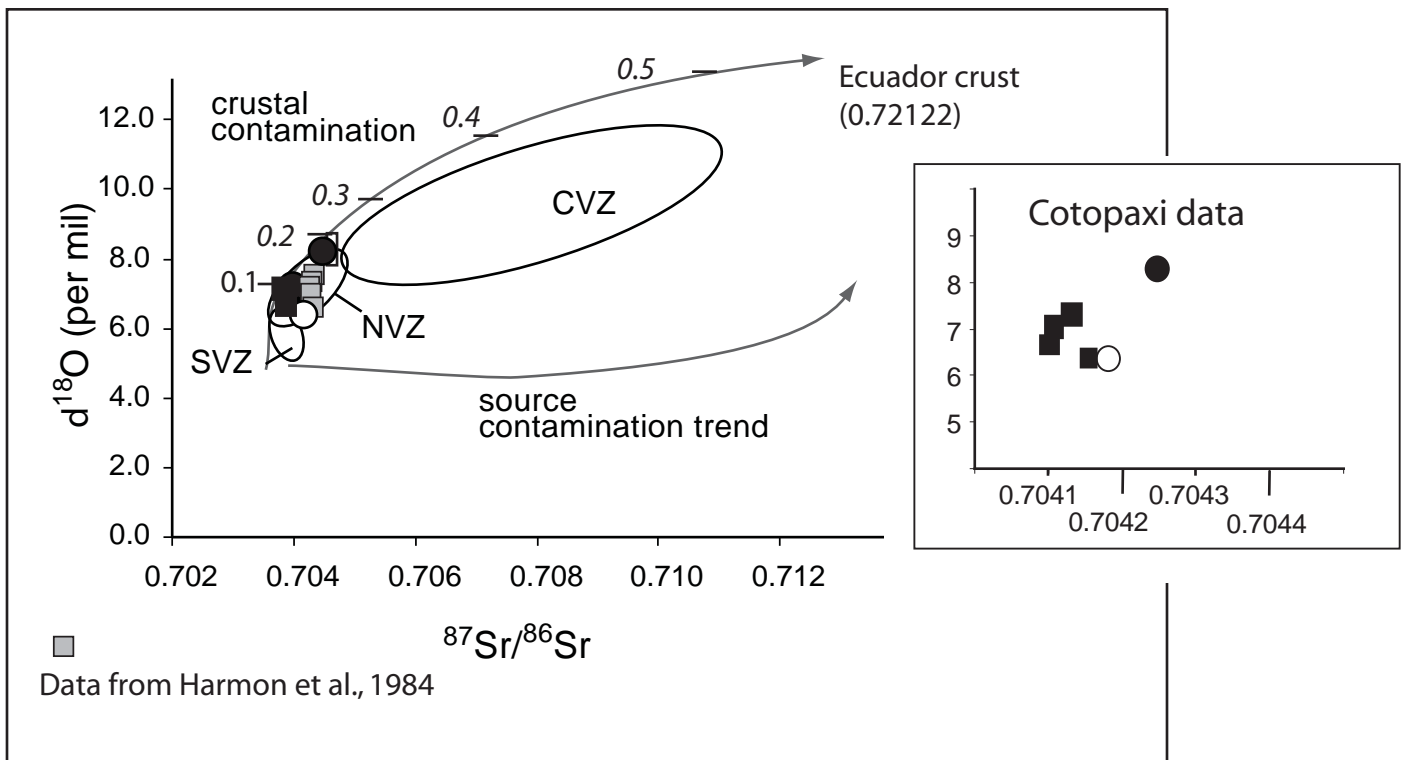


Figure 11

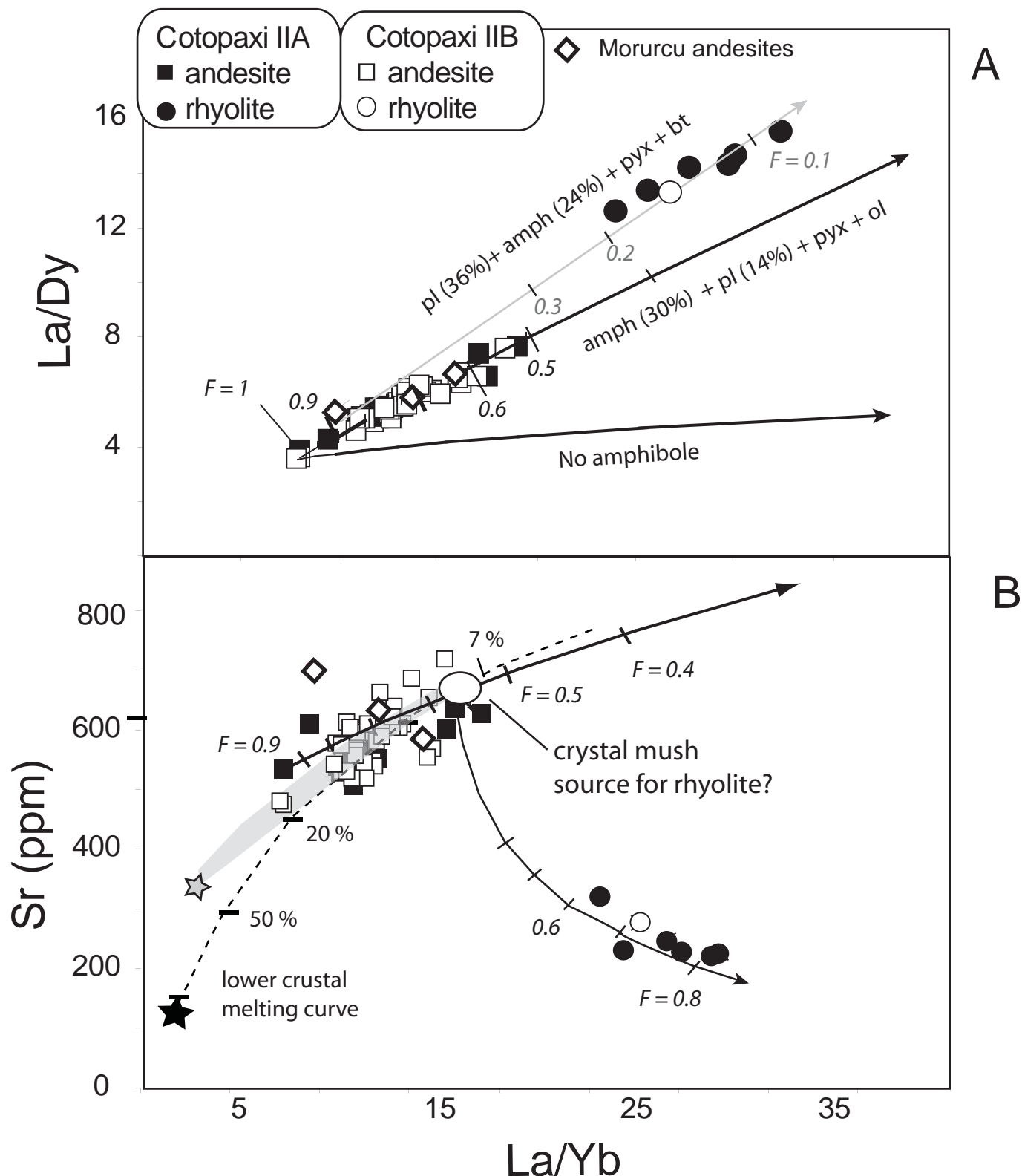


Figure 12

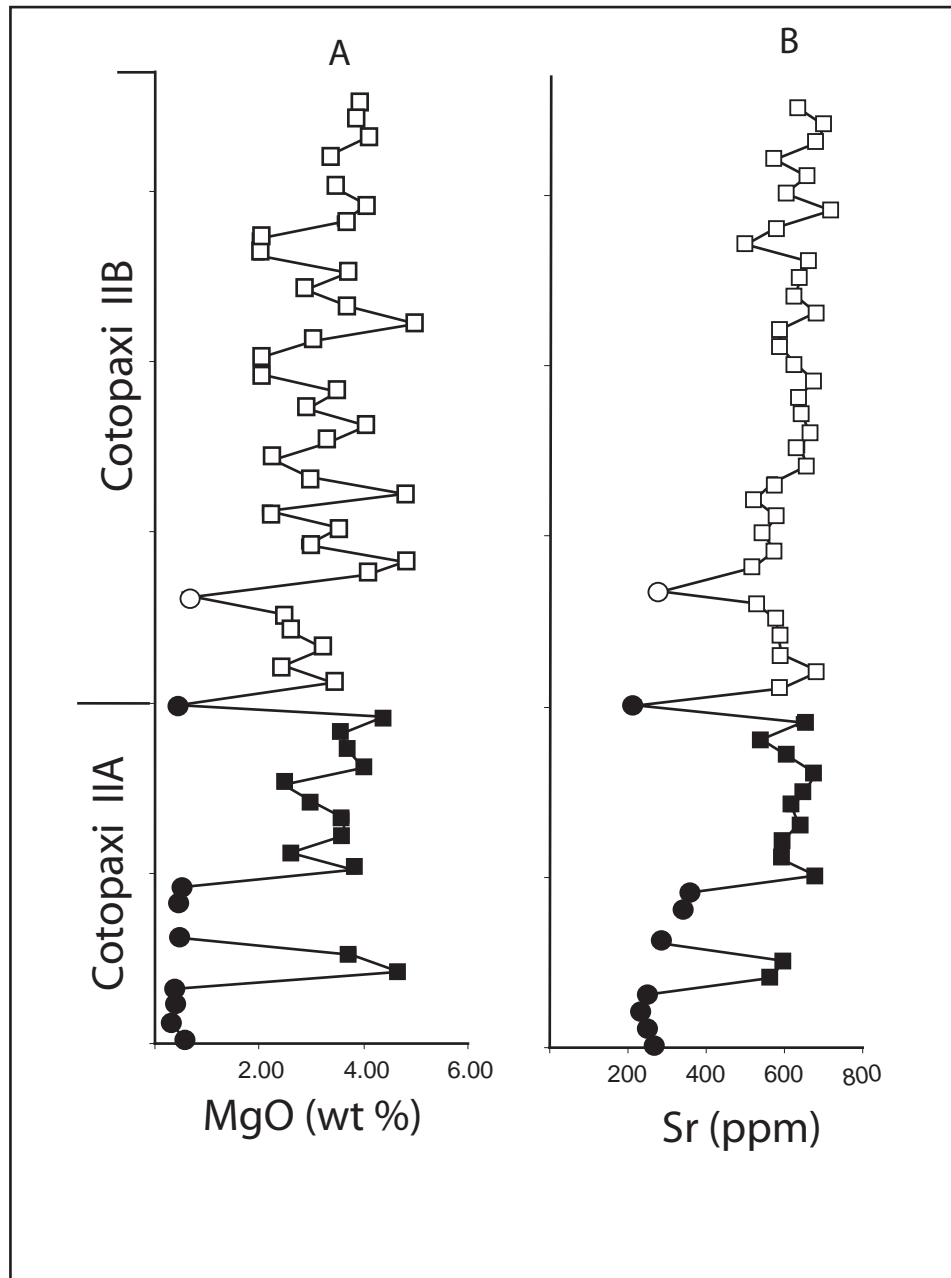


Figure 13

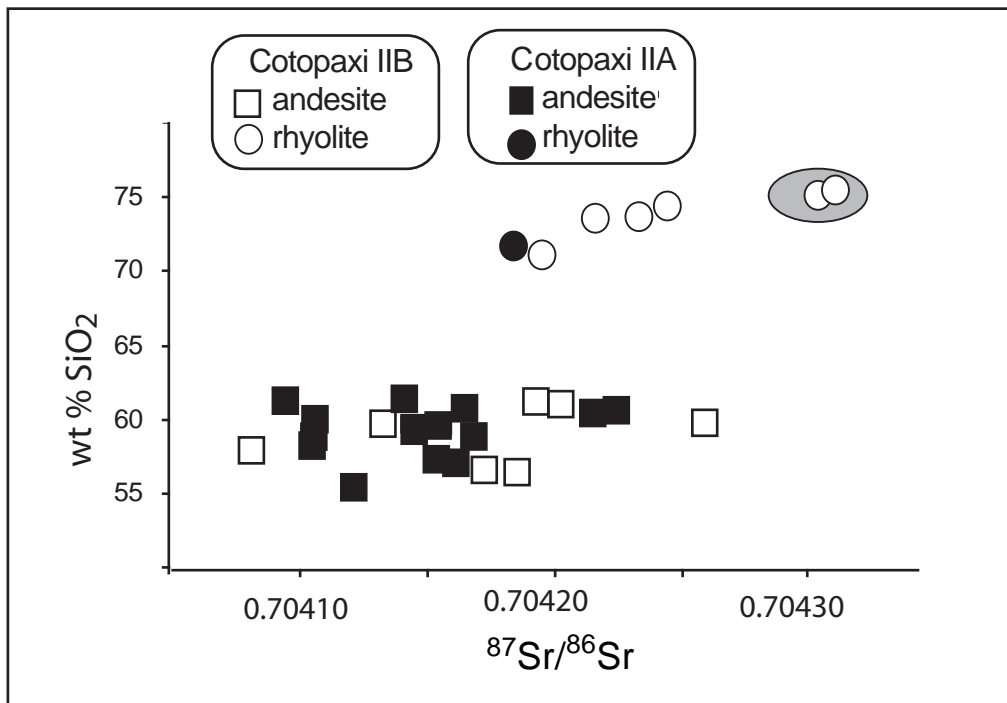


Figure 14

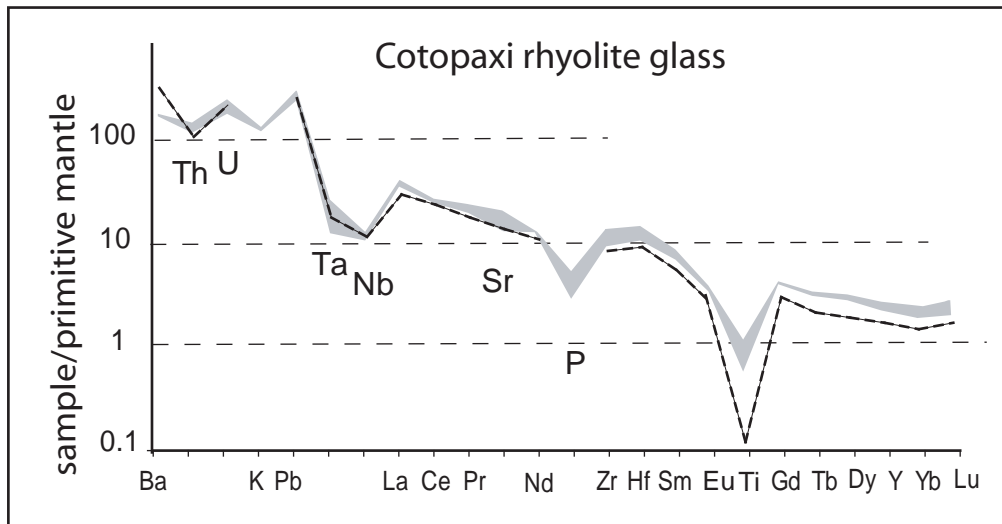


Figure 15

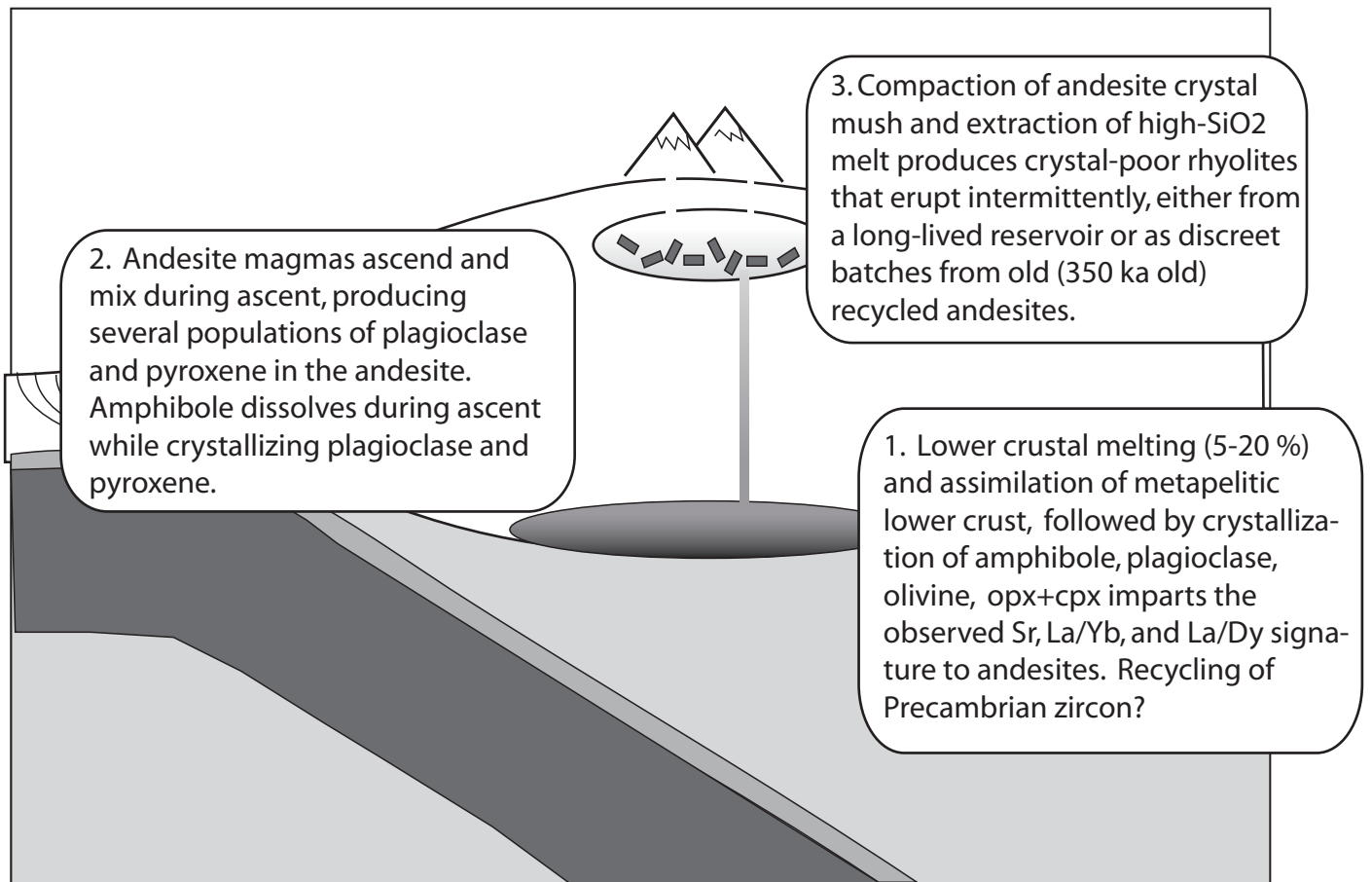


Table 1. Major, minor and trace element analyses of Cotopaxi whole rocks in stratigraphic order.*

	Cotopaxi I								Cotopaxi II A
	Chalupas CTX- 14	Chalupas CTX-36	Chalupas CTX-48	Chalupas CTX-86	Chalupas CTX-130	Morurcu CTX-77	Morurcu CTX-78	Morurcu CTX-82	F1 of "F" series CTX-67
SiO₂	72.68	73.30	73.28	73.36	71.30	62.52	60.89	61.13	72.65
Al₂O₃	13.94	13.85	14.35	13.89	14.80	17.90	18.42	18.04	14.23
TiO₂	0.237	0.24	0.25	0.23	0.26	0.661	0.696	0.604	0.163
FeO	1.22	1.25	1.32	1.19	1.35	4.96	5.52	5.43	1.42
MnO	0.043	0.05	0.05	0.04	0.05	0.087	0.091	0.103	0.058
CaO	1.22	1.15	1.23	1.20	1.23	5.46	6.22	6.33	1.49
MgO	0.24	0.31	0.31	0.28	0.34	2.23	2.47	2.77	0.41
K₂O	4.44	4.47	4.59	4.54	4.33	1.66	1.47	1.59	2.96
Na₂O	3.91	3.94	3.92	3.82	3.42	4.34	4.32	4.07	3.98
P₂O₅	0.042	0.04	0.05	0.06	0.06	0.238	0.234	0.200	0.057
Total	97.98	98.59	99.34	98.61	97.13	100.05	100.33	100.27	97.42
Ni	4	5	5	3	4	9	6	9	11
Cr	1	0	1	2	3	10	19	21	34
Sc	2.3	2.6	2.6	2.5	2.4	11.3	13.0		3.2
V	8	15	10	9	6	110	133	138	18
Ba	1056	1037	1075	1014	1056	644	578		954
Rb	174.6	175.4	175.9	172.8	167.2	38.3	32.9		71.4
Sr	223	204	213	202	187	576	609		248
Zr	178	172	193	180	193	127	112	105	85
Y	13.32	13.28	13.70	13.54	10.24	12.62	13.39		8.33
Nb	11.80	11.59	12.20	11.58	12.79	5.98	4.40		7.96
Pb	18.23	22.69	15.16	23.30	25.83	8.03	5.23		14.88
La	33.24	32.75	32.68	31.56	20.32	16.44	15.06		21.30
Ce	56.31	55.94	55.35	54.07	38.66	31.73	28.86		36.91
Th	23.56	22.37	23.02	22.41	19.37	3.99	3.51		8.32
Pr	5.73	5.71	5.77	5.54	4.26	3.87	3.54		3.85
Nd	19.37	19.65	19.86	19.36	15.15	16.29	15.12		13.59
Sm	3.34	3.62	3.65	3.44	2.92	3.71	3.47		2.53
Eu	0.66	0.66	0.67	0.64	0.54	1.10	1.07		0.55
Gd	2.57	2.64	2.68	2.55	2.18	3.30	3.14		1.94
Tb	0.39	0.41	0.41	0.40	0.33	0.46	0.46		0.27
Dy	2.24	2.37	2.31	2.35	1.96	2.50	2.59		1.50
Ho	0.43	0.45	0.46	0.45	0.39	0.46	0.50		0.28
Er	1.18	1.25	1.25	1.28	1.08	1.22	1.32		0.71
Tm	0.19	0.19	0.20	0.20	0.17	0.17	0.19		0.11
Yb	1.23	1.29	1.27	1.31	1.12	1.04	1.13		0.72
Lu	0.20	0.21	0.21	0.21	0.19	0.16	0.18		0.11
Hf	5.38	5.38	5.55	5.50	5.83	3.48	3.09		2.77
Ta	1.36	1.20	1.26	1.19	1.49	0.44	0.31		0.77
U	9.93	9.41	9.33	9.49	7.21	1.65	1.28		3.89

* Major elements and Ni, Cr, V and Zr were measured by XRF, all other trace elements were measured using ICP.

Table 1, continued

Cotopaxi IIA											
	F2 CTX-17	CTX CTX-18	CTX CTX-61	CTX CTX-62	CTX CTX-66	CTX CTX-60	CTX CTX-65B	CTX CTX-65A	F3 AF CTX-42	F3 PF CTX-43	F4 AF CTX-15
SiO₂	73.99	58.50	56.74	59.59	74.67	74.11	57.22	60.61	73.86	70.53	71.90
Al₂O₃	13.80	17.79	18.05	17.42	13.87	13.97	18.25	18.95	14.88	15.49	14.80
TiO₂	0.102	0.732	0.788	0.729	0.115	0.126	0.828	0.67	0.16	0.263	0.190
FeO	0.91	5.87	6.86	5.98	0.99	1.09	7.150	5.04	1.05	1.95	1.22
MnO	0.061	0.111	0.122	0.108	0.066	0.068	0.114	0.09	0.06	0.076	0.072
CaO	1.26	7.24	7.86	6.64	1.31	1.37	7.110	6.09	1.54	2.29	1.79
MgO	0.15	3.96	4.47	3.59	0.22	0.24	3.720	1.77	0.31	0.75	0.34
K₂O	3.03	1.21	1.14	1.44	3.01	2.97	1.280	1.78	2.80	2.58	2.78
Na₂O	4.32	3.94	3.89	4.11	4.26	4.34	4.090	4.52	4.59	4.21	4.64
P₂O₅	0.050	0.174	0.183	0.189	0.070	0.061	0.198	0.23	0.07	0.101	0.078
Total	97.67	99.53	100.11	99.79	98.58	98.34	99.96	99.75	99.33	98.24	97.81
Ni	4	17	13	17	5	5	19	4	5	8	1
Cr	0	79	54	82	1	0	38	9	0	34	1
Sc	2.2	19.4	22.0	18.8	2.2	2.5	24	8	2.3	4.0	2.2
V	15	161	178	142	2	3	168	109	4	26	14
Ba	969	523	463	589	983	920	526	695	1015	938	961
Rb	74.2	27.9	25.0	33.7	74.9	71.8	29	44	69.2	65.6	69.0
Sr	229	524	549	567	215	233	599	635	268	346	321
Zr	84	121	113	128	91	98	110	133	114	129	128
Y	8.48	14.67	15.93	14.80	8.70	8.59	16	16	9.03	10.03	9.61
Nb	7.30	4.03	3.91	4.78	7.28	6.94	5	6	7.34	6.81	6.95
Pb	14.80	6.61	5.62	7.21	14.67	13.46	6	9	16.25	13.52	13.39
La	22.65	12.53	11.21	14.14	22.76	20.37	13	17	22.03	21.00	22.03
Ce	38.56	24.32	21.92	27.41	39.38	35.37	26	33	37.64	37.68	38.29
Th	9.53	3.52	2.60	3.74	8.44	8.03	3	5	8.32	7.38	8.28
Pr	3.99	2.96	2.78	3.33	4.16	3.78	3	4	4.08	4.01	4.04
Nd	13.97	12.72	12.37	14.21	14.72	13.49	14	16	14.53	14.68	14.56
Sm	2.42	3.12	3.17	3.42	2.67	2.52	4	4	2.68	2.75	2.50
Eu	0.56	1.02	1.03	1.05	0.56	0.54	1	1	0.60	0.69	0.67
Gd	1.88	3.08	3.07	3.16	1.98	1.88	3	3	1.99	2.18	2.02
Tb	0.27	0.47	0.49	0.48	0.29	0.27	1	1	0.29	0.31	0.30
Dy	1.46	2.69	2.89	2.83	1.56	1.53	3	3	1.56	1.75	1.65
Ho	0.27	0.54	0.58	0.55	0.29	0.29	1	1	0.30	0.34	0.31
Er	0.70	1.44	1.54	1.47	0.79	0.77	2	1	0.79	0.92	0.84
Tm	0.11	0.21	0.22	0.21	0.12	0.12	0	0	0.12	0.14	0.13
Yb	0.70	1.29	1.41	1.30	0.76	0.76	1	1	0.79	0.92	0.86
Lu	0.11	0.21	0.22	0.21	0.12	0.12	0	0	0.13	0.15	0.15
Hf	2.67	3.10	2.96	3.41	2.99	2.96	3	4	3.33	3.61	3.60
Ta	0.84	0.28	0.27	0.34	0.67	0.65	0	0	0.65	0.58	0.57
U	4.03	1.31	0.93	1.40	3.47	3.38	1	2	3.23	2.98	3.23

Table 1, continued

	Cotopaxi IIA										
	F4 PF CTX-19	CTX CTX-112	CTX CTX-109	CTX CTX-111	CTX CTX-110	GF scoria ¹ CTX-40a	GF scoria ¹ CTX-40b	GF lava CTX-37	F5 CTX-41	CTX CTX-135	MSO ² CTX-30
SiO₂	71.84	58.41	59.76	56.71	56.71	60.95	60.40	60.85		58.09	59.98
Al₂O₃	15.13	17.15	18.18	18.44	18.44	18.39	19.10	16.86		17.82	17.56
TiO₂	0.207	0.835	0.681	0.84	0.843	0.77	0.73	0.75		0.794	0.694
FeO	1.58	6.59	5.27	7.32	7.32	5.15	4.98	5.63		6.45	6.02
MnO	0.076	0.096	0.088	0.11	0.114	0.09	0.09	0.09		0.111	0.103
CaO	2.01	6.56	5.93	7.04	7.04	5.42	5.40	6.18		6.69	6.39
MgO	0.42	3.61	2.43	3.44	3.44	2.28	2.41	3.82		3.53	3.40
K₂O	2.74	1.34	1.39	1.22	1.22	1.76	1.62	1.86		1.55	1.53
Na₂O	4.63	4.11	4.10	3.91	3.91	4.11	4.12	4.24		3.82	4.03
P₂O₅	0.093	0.235	0.218	0.19	0.194	0.26	0.25	0.23		0.200	0.178
Total	98.72	98.93	98.05	99.24	99.24	99.18	99.10	100.51		99.06	99.89
Ni	10	19	11	12	12	3	3	36		16	22
Cr	15	89	38	18	18	7	7	95		33	58
Sc	2.6	14.6	13.5	18.4	17.6	13.8	13.8	17.2	3	5.6	17.6
V	10	151	103	170	170	129	129	144		165	155
Ba	896	610	579	486	539	757	757	759	913	932	594
Rb	67.9	27.4	30.0	27.2	28.6	47.3	47.3	50.1	66	95.4	36.6
Sr	338	656	567	569	612	619	619	653	386	401	518
Zr	127	117	125	106	106	134	134	125		114	114
Y	10.00	12.43	13.73	15.67	14.80	14.07	14.07	13.28	11	18.96	14.66
Nb	6.74	5.54	5.13	4.32	4.48	6.25	6.25	6.10	7	9.35	4.38
Pb	12.85	6.87	7.59	6.00	7.18	10.15	10.15	9.54	12	20.19	7.37
La	20.80	16.44	14.93	12.72	14.58	20.50	20.50	19.64	21	30.39	14.34
Ce	36.98	31.60	28.49	25.11	27.88	38.17	38.17	36.09	37	53.21	27.63
Th	7.60	3.11	3.48	2.87	3.19	5.90	5.90	5.72	7	13.32	3.95
Pr	3.90	3.91	3.54	3.17	3.43	4.56	4.56	4.31	4	6.11	3.28
Nd	14.14	16.89	15.08	13.81	14.82	18.32	18.32	17.30	15	23.10	13.78
Sm	2.62	3.97	3.59	3.50	3.59	4.15	4.15	3.79	3	4.76	3.24
Eu	0.64	1.21	0.99	1.07	1.09	1.11	1.11	1.13	1	1.09	0.95
Gd	1.97	3.47	3.23	3.32	3.19	3.46	3.46	3.19	2	3.96	3.03
Tb	0.30	0.47	0.48	0.51	0.49	0.50	0.50	0.47	0.34	0.59	0.46
Dy	1.66	2.53	2.69	3.00	2.87	2.82	2.82	2.57	2	3.40	2.66
Ho	0.32	0.47	0.50	0.60	0.55	0.53	0.53	0.47	0.38	0.67	0.53
Er	0.85	1.18	1.28	1.59	1.44	1.38	1.38	1.27	1	1.83	1.39
Tm	0.13	0.16	0.18	0.22	0.20	0.19	0.19	0.18	0.16	0.26	0.20
Yb	0.87	0.94	1.14	1.35	1.24	1.22	1.22	1.03	1	1.66	1.21
Lu	0.15	0.14	0.18	0.21	0.19	0.19	0.19	0.16	0	0.27	0.19
Hf	3.33	3.11	3.30	2.87	2.84	3.61	3.61	3.32	4	5.42	3.01
Ta	0.55	0.35	0.35	0.29	0.30	0.43	0.43	0.41	1	0.77	0.30
U	2.89	1.06	1.24	0.96	1.11	1.86	1.86	1.70	3	4.26	1.30

1 . GF is a regional marker unit

2. MSO - Mariann Smith outcrop - soil dated here at 4420 +- 80 years BP

Table 1, continued

	Colorado Canyon Series						Cotopaxi IIB				
	MSO	CC	CC	CC	CC	CC	I AF	lava A	J PF	J AF	lava A
	CTX-29	CTX-72	CTX-73	CTX-74	CTX-27a	CTX-27b	CTX-16	CTX-51	CTX-49a	CTX-50	CTX-107
SiO₂	57.77	73.20	74.96	74.63	72.59	72.67	59.92	60.83	61.16	61.58	59.84
Al₂O₃	17.49	14.05	13.42	13.81	13.68	13.83	17.03	18.44	17.23	18.10	18.22
TiO₂	0.816	0.244	0.234	0.112	0.234	0.236	0.752	0.773	0.705	0.669	0.76
FeO	6.54	1.27	1.19	1.01	1.30	1.26	5.78	5.47	5.72	5.28	5.92
MnO	0.109	0.048	0.043	0.063	0.046	0.046	0.097	0.085	0.096	0.089	0.10
CaO	7.09	1.20	1.10	1.24	1.17	1.21	6.16	6.30	5.88	5.97	6.52
MgO	4.19	0.32	0.31	0.21	0.27	0.27	3.24	2.28	3.07	2.42	2.77
K₂O	1.42	4.70	4.16	3.07	4.58	4.58	1.56	1.49	1.68	1.41	1.56
Na₂O	4.00	3.42	3.12	4.19	3.37	3.42	4.09	4.50	4.33	4.48	4.29
P₂O₅	0.230	0.060	0.056	0.067	0.036	0.039	0.209	0.241	0.205	0.206	0.22
Total	99.66	98.51	98.59	98.40	97.27	97.56	98.84	100.41	100.07	100.20	100.20
Ni	35	6	6	4	4	6	10	8	18	10	64
Cr	69	0	4	0	0	0	47	27	55	26	243
Sc	20.0	2.4	2.4	2.1		2.2	14.5	11.8	13.1	13.4	14.8
V	162	11	11	10	20	10	140	125	123	110	123
Ba	594	1058	962	974		1052	667	647	693	611	607
Rb	32.9	173.8	153.8	79.6		163.1	36.9	29.5	41.2	30.0	35.0
Sr	619	204	188	206		182	569	663	569	561	593
Zr	118	181	175	86	174	177	123	124	125	120	121
Y	16.27	13.52	12.78	8.42		10.58	13.84	13.94	13.58	14.24	14.29
Nb	5.32	11.83	11.31	7.35		11.86	5.61	5.90	5.46	4.96	5.16
Pb	7.19	22.81	19.10	14.69		24.79	8.10	7.12	8.39	6.94	7.47
La	16.52	32.98	31.43	22.33		23.30	17.75	16.88	17.60	14.98	16.09
Ce	31.57	56.74	53.57	38.39		43.52	33.30	32.40	32.95	31.60	30.74
Th	3.93	22.47	21.47	8.55		19.44	4.80	3.31	4.87	3.30	3.79
Pr	3.81	5.83	5.56	4.04		4.58	3.95	4.01	3.93	3.62	3.75
Nd	16.12	20.15	18.91	14.41		15.89	16.21	17.14	16.46	15.23	15.86
Sm	3.79	3.63	3.46	2.63		3.00	3.74	3.97	3.78	3.70	3.79
Eu	1.13	0.69	0.65	0.54		0.54	1.14	1.19	1.11	1.03	1.12
Gd	3.47	2.67	2.58	1.91		2.22	3.31	3.49	3.28	3.26	3.40
Tb	0.52	0.41	0.40	0.27		0.35	0.49	0.49	0.49	0.49	0.51
Dy	3.02	2.36	2.22	1.53		2.02	2.67	2.68	2.73	2.69	2.81
Ho	0.59	0.45	0.44	0.28		0.40	0.50	0.49	0.51	0.51	0.54
Er	1.54	1.28	1.21	0.74		1.11	1.26	1.24	1.30	1.31	1.40
Tm	0.22	0.20	0.19	0.11		0.18	0.18	0.17	0.18	0.19	0.20
Yb	1.33	1.30	1.23	0.72		1.14	1.08	1.05	1.10	1.15	1.20
Lu	0.21	0.21	0.20	0.12		0.19	0.17	0.16	0.17	0.18	0.19
Hf	3.07	5.67	5.43	2.82		5.43	3.29	3.32	3.37	3.22	3.21
Ta	0.35	1.22	1.17	0.69		1.73	0.38	0.39	0.40	0.33	0.35
U	1.36	9.39	9.27	3.59		8.17	1.69	1.13	1.71	1.15	1.25

3. Soil above this unit dated at 2050 +- 80 BP

Table 1, continued.

Cotopaxi IIB											
	JK AF ² CTX-53a	JK AF ³ CTX-53b	CTX ⁴ CTX-103	CTX CTX-104	CTX CTX-106	CTX CTX-102	CTX CTX-101	CTX CTX-99	lava A CYX-108	CTX CYX-96	lava A CTX-95
SiO₂	57.67	57.04	61.25	58.50	57.18	59.52	58.97	61.14	59.47	57.58	57.29
Al₂O₃	16.90	17.40	17.65	16.74	17.38	17.70	17.63	18.21	17.99	18.19	19.37
TiO₂	0.761	0.746	0.666	0.765	0.75	0.702	0.764	0.702	0.76	0.83	0.69
FeO	7.34	7.22	5.26	6.88	7.00	6.30	6.68	4.82	5.84	7.28	5.39
MnO	0.118	0.114	0.088	0.110	0.11	0.105	0.109	0.082	0.09	0.12	0.09
CaO	7.92	7.57	5.94	6.72	7.55	6.14	6.62	5.93	6.46	7.00	7.84
MgO	4.10	4.52	2.31	4.33	4.59	2.75	3.36	2.01	2.80	3.48	3.20
K₂O	0.97	0.99	1.44	1.19	0.99	1.44	1.36	1.74	1.52	1.46	1.26
Na₂O	3.77	3.92	4.32	3.84	3.62	4.15	4.01	4.45	4.29	4.05	3.99
P₂O₅	0.182	0.178	0.205	0.195	0.17	0.202	0.214	0.225	0.21	0.21	0.19
Total	99.73	99.70	99.13	99.27	99.34	99.01	99.71	99.31	99.43	100.20	99.31
Ni	28	29	8	31	30	10	17	12	20		
Cr	77	73	26	129	80	32	29	36	46		
Sc	23.1	22.7	12.7	17.6	22.0	14.3	15.7	11.2	14.7	18.7	16.2
V	165	177	104	163	169	136	155	105	126		
Ba	357	387	604	507	405	592	569	688	623	608	544
Rb	20.9	20.7	30.7	24.5	21.3	32.7	31.0	40.6	35.2	35.7	26.9
Sr	502	497	554	532	496	551	522	620	603	610	764
Zr	98	95	121	108	94	118	114	132	122		
Y	15.10	14.49	13.53	12.87	14.72	14.49	14.41	15.12	14.56	15.10	11.80
Nb	3.80	3.57	5.06	4.30	3.47	4.87	5.27	5.88	5.20	4.78	4.57
Pb	4.69	4.69	7.88	6.88	5.02	8.16	7.78	9.35	6.39	8.23	7.32
La	9.32	9.55	14.62	12.92	10.05	14.16	14.37	18.01	16.28	15.58	14.30
Ce	18.80	19.45	28.18	25.35	20.63	27.43	27.91	34.19	31.14	29.81	27.10
Th	2.23	2.14	3.12	2.55	2.12	3.29	3.08	4.38	3.83	3.98	3.41
Pr	2.45	2.47	3.47	3.16	2.61	3.40	3.48	4.15	3.86	3.63	3.29
Nd	11.30	10.97	14.76	13.82	11.82	14.56	14.85	17.36	16.28	15.38	13.82
Sm	2.90	2.95	3.59	3.44	3.13	3.57	3.67	3.97	3.83	3.73	3.23
Eu	0.94	0.94	1.06	1.00	0.94	1.03	1.06	1.17	1.17	1.10	1.05
Gd	2.94	2.94	3.17	3.11	3.07	3.29	3.29	3.48	3.42	3.31	2.88
Tb	0.48	0.46	0.49	0.46	0.47	0.49	0.50	0.52	0.51	0.51	0.42
Dy	2.66	2.72	2.68	2.60	2.79	2.79	2.88	2.91	2.86	2.99	2.34
Ho	0.57	0.53	0.51	0.49	0.54	0.53	0.53	0.56	0.56	0.57	0.44
Er	1.41	1.42	1.27	1.22	1.43	1.41	1.36	1.47	1.46	1.46	1.11
Tm	0.19	0.20	0.19	0.17	0.21	0.20	0.20	0.20	0.20	0.21	0.16
Yb	1.30	1.24	1.11	1.03	1.25	1.27	1.20	1.28	1.21	1.27	0.94
Lu	0.19	0.20	0.18	0.16	0.20	0.20	0.19	0.20	0.20	0.20	0.15
Hf	2.20	2.56	3.14	2.82	2.57	3.15	3.09	3.57	3.24	3.02	2.58
Ta	0.26	0.24	0.91	0.29	0.22	0.35	1.11	0.40	0.35	0.33	0.30
U	0.73	0.75	1.21	0.97	0.75	1.29	1.19	1.51	1.27	1.31	1.09

4. Samples 103 - 99 collected on east side of Colorado Canyon, Fig. A1

Table 1, continued.

Cotopaxi IIB												
	CTX CTX-98	CTX CTX-97	PB ⁵ CTX-90	PB CTX-91	PB CTX-92	PB CTX-93	PB CTX-94	KA1 CTX-25	KA2 CTX-23	KB1 CTX-21	lava B CTX-47	lava B CTX-46
SiO₂	58.77	56.99	68.57	61.32	60.01	61.03	73.26	59.18	59.40	57.37	59.85	61.31
Al₂O₃	17.85	17.95	15.44	17.84	17.70	18.59	14.88	18.17	18.62	18.30	17.96	17.81
TiO₂	0.70	0.87	0.278	0.679	0.697	0.71	0.16	0.795	0.732	0.822	0.77	0.66
FeO	6.73	6.78	2.06	5.23	6.16	4.40	1.05	6.19	5.55	7.13	6.07	5.57
MnO	0.12	0.12	0.081	0.091	0.103	0.08	0.06	0.108	0.100	0.111	0.10	0.10
CaO	6.53	7.21	2.55	5.99	6.10	6.01	1.54	6.42	6.66	6.90	6.46	6.02
MgO	3.06	3.99	0.69	2.38	2.78	2.10	0.31	3.14	2.74	3.31	2.90	2.85
K₂O	1.40	1.27	2.48	1.40	1.46	1.69	2.80	1.60	1.63	1.47	1.55	1.49
Na₂O	4.20	3.91	4.50	4.13	4.01	4.30	4.59	4.18	4.13	4.05	4.48	4.27
P₂O₅	0.23	0.26	0.132	0.214	0.203	0.22	0.07	0.212	0.194	0.204	0.22	0.19
Total	99.59	99.34	96.78	99.27	99.23	99.14	99.33	99.99	99.76	99.67	100.35	100.27
Ni			4	7	8	10.00	5	7	8	12		
Cr			4	27	19	20.00	0	16	21	19		
Sc	14.9	18.5		12.5	15.0	11.00	2.3	16.8	16.6	19.9	14.9	13.3
V			17	114	134	104.00	4	160	140	175		
Ba	578	540		585	582	659.60	1015	658	659	599	620	589
Rb	31.3	25.6		30.0	33.8	38.84	69.2	37.5	41.0	36.1	35.6	34.2
Sr	605	693		505	547	634.64	268	615	620	610	590	594
Zr			143	121	119	134.00	114	122	115	113		
Y	15.64	14.81		13.49	14.45	14.63	9.03	15.61	14.86	15.90	15.34	13.65
Nb	4.93	5.41		5.13	4.87	5.74	7.34	5.62	4.82	4.96	5.20	4.94
Pb	7.52	6.32		7.97	7.42	8.64	16.25	7.76	8.32	7.30	6.55	6.67
La	14.89	15.57		14.33	14.02	17.32	22.03	17.72	15.48	15.17	16.39	14.31
Ce	28.99	30.53		29.32	27.06	33.30	37.64	33.52	29.66	29.17	31.48	27.77
Th	3.14	2.94		3.22	3.43	4.36	8.32	4.53	4.67	4.07	3.96	3.74
Pr	3.59	3.80		3.46	3.34	4.00	4.08	3.98	3.55	3.52	3.89	3.45
Nd	15.49	16.55		14.68	14.36	16.75	14.53	16.78	14.78	15.14	16.77	14.95
Sm	3.71	3.87		3.59	3.47	3.88	2.68	3.89	3.38	3.57	3.97	3.61
Eu	1.10	1.18		1.01	1.02	1.13	0.60	1.16	1.04	1.08	1.18	1.09
Gd	3.34	3.53		3.25	3.22	3.40	1.99	3.43	3.10	3.31	3.55	3.25
Tb	0.53	0.52		0.48	0.49	0.51	0.29	0.51	0.47	0.50	0.53	0.49
Dy	2.95	2.99		2.77	2.80	2.89	1.56	2.96	2.65	2.83	3.03	2.73
Ho	0.59	0.55		0.50	0.54	0.54	0.30	0.56	0.52	0.54	0.57	0.52
Er	1.50	1.44		1.31	1.42	1.39	0.79	1.43	1.35	1.41	1.48	1.31
Tm	0.21	0.20		0.18	0.20	0.19	0.12	0.21	0.19	0.20	0.21	0.19
Yb	1.34	1.20		1.14	1.24	1.20	0.79	1.26	1.18	1.24	1.25	1.14
Lu	0.21	0.19		0.18	0.20	0.19	0.13	0.20	0.19	0.20	0.19	0.18
Hf	3.11	2.93		3.23	3.15	3.47	3.33	3.38	3.02	3.00	3.26	3.21
Ta	0.34	0.33		0.82	0.35	0.39	0.65	0.38	0.32	0.32	0.35	0.39
U	1.17	0.97		1.15	1.29	1.43	3.23	1.48	1.48	1.30	1.34	1.62

5. PB = Penas Blancas - location on Fig. A1

Table 1, continued.

Cotopaxi IIB												
L unit	CTX	X unit	MZ	MZ	CTX	lava B	CTX ⁶	CTX	CTX	CTX	CTX	CTX
CTX-22	CTX-24	CTX-26	CTX-34M	CTX-34Z	CTX-120	CTX-119	CTX-116	CTX-117	CTX-118	CTX-126b	CTX-123	
SiO₂	59.82	57.16	60.50	62.75	57.49	58.24	59.60	59.84	57.17	58.17	58.88	59.95
Al₂O₃	19.14	18.14	19.09	17.43	18.21	17.67	18.00	17.87	18.41	19.41	18.20	19.04
TiO₂	0.724	0.824	0.686	0.524	0.832	0.69	0.772	0.765	0.831	1.831	0.723	0.689
FeO	5.02	6.79	5.11	5.04	7.09	6.59	5.81	5.87	7.06	8.06	6.09	4.93
MnO	0.089	0.114	0.092	0.110	0.112	0.12	0.095	0.096	0.116	1.116	0.098	0.090
CaO	6.37	7.26	6.13	5.30	6.91	6.62	6.47	6.47	7.16	8.16	6.49	6.22
MgO	1.91	3.86	1.83	1.81	3.43	3.17	2.87	2.90	3.55	4.55	2.70	1.85
K₂O	1.76	1.39	1.76	1.69	1.48	1.36	1.53	1.53	1.32	2.32	1.64	1.77
Na₂O	4.37	3.95	4.39	4.16	4.01	3.95	4.22	4.22	4.03	5.03	3.94	4.22
P₂O₅	0.230	0.204	0.232	0.239	0.210	0.22	0.219	0.216	0.210	1.210	0.197	0.234
Total	99.43	99.69	99.82	99.05	99.78	98.64	99.58	99.78	99.86	100.86	98.96	98.99
Ni	2	15	2	4	9		17	19	12	13	7	3
Cr	10	38	7	15	34		47	44	34	35	15	9
Sc	13.5	21.2	11.6	8.9	17.8	15.4	15.4	15.2	17.7	18.7	15.5	12.2
V	112	173	101	83	172		139	154	171	172	149	91
Ba	706	582	670	681	615	564	594	604	571	572	667	723
Rb	43.9	32.4	41.5	41.2	35.6	31.3	34.8	35.4	30.2	31.2	42.6	44.2
Sr	652	639	602	478	556	618	564	586	656	657	604	636
Zr	132	109	134	135	114		121	121	112	113	118	132
Y	16.03	15.47	15.65	15.15	15.22	15.67	14.73	14.81	15.67	16.67	14.28	15.59
Nb	5.81	4.77	5.46	5.09	4.96	4.95	5.20	5.18	4.77	5.77	4.73	5.65
Pb	8.83	6.96	8.36	9.35	8.46	6.64	7.44	7.59	7.65	8.65	8.47	8.89
La	18.22	15.17	17.41	15.96	15.94	14.50	15.76	15.89	15.35	16.35	16.00	18.82
Ce	34.99	29.32	33.33	30.24	30.54	28.03	30.09	30.40	29.38	30.38	29.75	35.30
Th	5.04	3.83	5.06	4.15	4.12	3.28	3.90	3.83	3.41	4.41	4.69	5.17
Pr	4.17	3.62	3.96	3.66	3.76	3.52	3.68	3.73	3.64	4.64	3.54	4.18
Nd	17.31	15.34	16.41	15.11	15.76	14.99	15.70	15.92	15.54	16.54	14.97	17.58
Sm	3.98	3.62	3.73	3.54	3.76	3.69	3.74	3.79	3.83	4.83	3.50	4.01
Eu	1.13	1.10	1.07	1.03	1.12	1.10	1.07	1.13	1.17	2.17	1.03	1.17
Gd	3.46	3.25	3.31	3.15	3.36	3.40	3.42	3.39	3.47	4.47	3.16	3.43
Tb	0.52	0.51	0.50	0.48	0.52	0.51	0.51	0.50	0.53	1.53	0.48	0.53
Dy	2.96	2.86	2.86	2.86	2.99	2.97	2.91	2.91	3.05	4.05	2.69	3.03
Ho	0.56	0.56	0.55	0.55	0.57	0.57	0.54	0.56	0.59	1.59	0.52	0.59
Er	1.46	1.45	1.47	1.46	1.49	1.52	1.40	1.46	1.47	2.47	1.43	1.55
Tm	0.20	0.20	0.21	0.21	0.21	0.22	0.20	0.20	0.22	1.22	0.20	0.22
Yb	1.28	1.21	1.29	1.35	1.32	1.33	1.19	1.23	1.33	2.33	1.19	1.34
Lu	0.20	0.20	0.21	0.23	0.21	0.21	0.19	0.19	0.20	1.20	0.19	0.21
Hf	3.35	2.91	3.35	3.54	3.09	3.05	3.16	3.19	3.06	4.06	3.17	3.52
Ta	0.39	0.30	0.37	0.50	0.41	0.33	0.35	0.35	0.32	1.32	0.33	0.40
U	1.61	1.19	1.63	1.47	1.33	1.16	1.30	1.27	1.16	2.16	1.50	1.64

6. Samples 116-124 collected beneath Yanashatcha D-type lava flow.

Table 1, continued.

Cotopaxi IIB											basement samples ⁷	
	CTX CTX-124	lava D CTX-75	M lower CTX-20b	M upper CTX-20a	CTX CTX-122	CTX CTX-125	CTX CTX-132	N unit CTX-128	1877 BP CTX-28a	1877 BP CTX-28b	CTX 114 metapelite	CTX 115 greenschist
SiO₂	57.17	57.17	58.70	56.59	56.64	58.54	57.60	56.38	57.59	57.32	92.79	48.73
Al₂O₃	18.06	18.06	17.92	18.10	17.92	17.81	18.09	17.88	17.59	16.79	2.56	15.13
TiO₂	0.828	0.828	0.694	0.867	0.886	0.697	0.821	0.905	0.801	0.798	0.341	1.369
FeO	7.19	7.19	6.22	7.01	7.12	6.66	6.83	7.07	7.21	6.99	4.04	8.62
MnO	0.115	0.115	0.120	0.120	0.116	0.119	0.116	0.112	0.116	0.116	0.039	0.190
CaO	7.06	7.06	6.58	7.18	7.11	6.61	7.11	7.17	7.02	7.14	0.13	9.12
MgO	3.51	3.51	3.21	3.90	3.86	3.26	3.60	3.68	3.74	4.24	0.11	7.08
K₂O	1.43	1.43	1.38	1.28	1.36	1.37	1.29	1.42	1.39	1.56	0.46	0.27
Na₂O	3.90	3.90	4.14	4.05	4.02	4.01	4.21	4.10	4.02	3.89	0.24	4.45
P₂O₅	0.204	0.204	0.222	0.254	0.262	0.224	0.206	0.274	0.220	0.230	0.032	0.166
Total	99.47	99.47	99.19	99.35	99.30	99.88	98.99	99.69	99.07	100.74	95.13	
Ni	13	13	13	20	21	15	15	18	22	22	16	103
Cr	20	20	41	43	36	43	29	54	37	37	92	180
Sc	18.6	14.6	15.5	19.5	17.3	15.3	17.3	15.6	18.7	18.7	2.2	35.1
V	179	179	137	170	157	127	169	168	164	164	19	225
Ba	588	602	508	560	583	545	536	621	577	577	76	120
Rb	35.6	35.2	28.0	26.3	27.2	29.0	28.8	28.3	31.5	31.5	17.1	3.1
Sr	617	520	550	659	695	578	633	677	614	614	16	208
Zr	111	111	112	112	119	116	107	124	114	114	339	91
Y	15.43	16.65	14.38	14.94	14.31	14.65	15.06	14.26	15.42	15.42	9.42	27.82
Nb	4.82	4.84	4.44	5.57	5.55	4.59	4.61	6.12	5.14	5.14	7.26	4.05
Pb	7.22	6.71	5.81	6.31	6.56	6.21	5.49	8.01	6.86	6.86	5.68	4.72
La	15.63	14.68	12.99	16.19	17.29	14.09	14.60	18.83	16.09	16.09	10.07	5.29
Ce	29.42	28.57	24.72	31.46	33.51	27.29	28.07	36.08	31.01	31.01	19.15	13.08
Th	4.06	3.58	2.87	2.94	3.37	3.11	3.26	3.55	3.76	3.76	3.59	0.59
Pr	3.54	3.57	3.09	3.79	4.10	3.36	3.48	4.40	3.73	3.73	2.12	1.94
Nd	15.33	15.42	13.36	16.52	17.60	14.50	14.82	18.85	15.84	15.84	8.09	10.03
Sm	3.68	3.72	3.23	4.00	4.11	3.54	3.60	4.29	3.72	3.72	1.76	3.45
Eu	1.13	1.12	1.03	1.20	1.22	1.08	1.11	1.27	1.14	1.14	0.33	1.50
Gd	3.33	3.51	2.97	3.41	3.55	3.14	3.29	3.64	3.43	3.43	1.56	4.26
Tb	0.51	0.54	0.45	0.51	0.51	0.49	0.51	0.52	0.51	0.51	0.26	0.79
Dy	2.90	3.07	2.56	2.94	2.92	2.83	2.86	2.89	3.00	3.00	1.59	5.04
Ho	0.57	0.62	0.50	0.55	0.55	0.56	0.56	0.53	0.57	0.57	0.34	1.05
Er	1.49	1.63	1.28	1.34	1.41	1.43	1.45	1.32	1.46	1.46	1.00	2.83
Tm	0.21	0.24	0.19	0.19	0.19	0.20	0.20	0.19	0.21	0.21	0.16	0.41
Yb	1.30	1.50	1.15	1.20	1.14	1.28	1.25	1.11	1.26	1.26	1.07	2.50
Lu	0.20	0.23	0.19	0.19	0.18	0.20	0.20	0.18	0.20	0.20	0.19	0.39
Hf	3.00	3.29	2.71	2.99	3.07	2.92	2.88	3.22	3.04	3.04	8.59	2.19
Ta	0.32	0.34	0.29	0.35	0.35	0.32	0.30	0.48	0.33	0.33	2.44	0.38
U	1.29	1.28	0.99	0.97	1.06	1.07	1.05	1.16	1.25	1.25	1.01	0.19

7. Basement samples collected near Tungurahua Volcano, north of Banos.

Table 2. Cotopaxi Sr, Nd and Pb* isotopes

sample	$^{87}\text{Sr}/^{86}\text{Sr}$	2σ	Sr	$^{143}\text{Nd}/^{144}\text{Nd}$	2σ	Nd	$^{208}\text{Pb}/^{204}\text{Pb}$	2σ	$^{207}\text{Pb}/^{204}\text{Pb}$	2σ	$^{206}\text{Pb}/^{204}\text{Pb}$	2σ	Pb	SiO_2
		$\times 10^{-5}$	ppm		$\times 10^{-5}$	ppm							ppm	(wt %)
rhyolite														
CH 99-14	0.70443	10	223	0.51282	10	19.4	38.825	0.005	15.650	0.004	18.981	0.004	18.2	72.7
CTX 99-15	0.70419	11	321	0.51282	9	14.6								71.9
CTX 99-17	0.70424	10	229	0.51281	9	14.0								74.0
CTX 99-19	0.70418	11	338	0.51286	10	14.1	38.650	0.005	15.602	0.005	18.932	0.004	12.9	71.8
CTX 99-60	0.70424	10	233			13.5								74.1
CTX 99-66			215			14.7	38.762	0.004	15.640	0.003	18.970	0.003	14.7	74.7
CTX 99-67							38.644	0.008	15.600	0.008	18.933	0.007		
CC 99-27B	0.70440	13	224	0.51272	10	19.2								72.7
CTX 99-35	0.70440	13	210	0.51276		19.8								73.7
CTX 99-36	0.70446	10	217	0.51284	7	22.1	38.781	0.005	15.639	0.004	18.968	0.004	24.2	73.3
CTX 99-42	0.70421	11	268	0.51279	17	14.5								73.9
CTX 99-69			230	0.513	7.000	14.8								74.2
CTX 99-72			204			20.2	38.769	0.007	15.627	0.007	18.962	0.007	22.8	73.2
andesite														
CTX 99-16	0.70426	15	569	0.51280	12	16.2								59.9
CTX 99-18	0.70408	15	524	0.51285	11	12.7								58.5
CTX 99-20A	0.70418	10	659	0.51286	12	16.5	38.823	0.008	15.654	0.007	18.955	0.006	6.3	56.6
CTX 99-20B	0.70410	11	550	0.51285	9	13.4								58.7
CTX 99-21	0.70416	11	610	0.51288	10	15.1								57.4
CTX 99-22	0.70413	13	652	0.51280	11	17.3								59.8
CTX 99-23	0.70417	10	620			14.8								59.4
CTX 99-24	0.70417	11	639	0.51282	9	15.3								57.2
CTX 99-25	0.70411	9	615	0.51282	11	16.8								59.2
CTX 99-26	0.70410	9	602	0.51252	9	16.4	38.696	0.013	15.617	0.010	18.923	0.008	8.4	60.5
CTX 99-28B	0.70415	11	614	0.51281	11	15.8	38.737	0.010	15.617	0.015	18.937	0.012	6.9	57.6
CTX 99-29	0.70415	11	619	0.51283	12	16.1	38.664	0.006	15.608	0.005	18.907	0.004	7.2	57.8

Table 2, continued

sample	$^{87}\text{Sr}/^{86}\text{Sr}$	2σ $\times 10^{-3}$	Sr ppm	$^{143}\text{Nd}/^{144}\text{Nd}$	2σ $\times 10^{-5}$	Nd ppm	$^{208}\text{Pb}/^{204}\text{Pb}$	2σ	$^{207}\text{Pb}/^{204}\text{Pb}$	2σ	$^{206}\text{Pb}/^{204}\text{Pb}$	2σ	Pb ppm	SiO_2 (wt %)	
CTX 99-30	0.70415	11	518			13.8									60.0
CTX 99-31	0.70412	11	636			20.6									55.9
CTX 99-34Z			594												57.5
CTX 99-37	0.70422	10	653	0.51275	8	17.3			38.678	0.005	15.614	0.005	18.827	0.005	9.0
CTX 99-39	0.70414	11	443			16.6									68.4
CTX 99-40A	0.70423	18	629	0.51278	12	18.4									61.0
CTX 99-40B			406	0.51282	10	15.4									71.2
CTX 99-41	0.70417	11	386	0.51282	8	15.4									
CTX 99-46	0.70409	11	594			15.0									61.3
CTX 99-47	0.70415	10	590	0.51284	10	16.8									59.9
CTX 99-49A	0.70420	10	569	0.51281	7	16.5									61.2
CTX 99-49B	0.70419	10	573	0.51280	9	16.5									61.4
CTX 99-50	0.70414	11	561	0.51283	7	15.2									61.6
CTX 99-51A	0.70416	10	663	0.51283	8	17.1									60.8
CTX 99-53A			499	0.51285	16	11.1									57.2
CTX 99-53B			497	0.51283	10	11.0	38.699	0.007	15.626	0.006	18.944	0.005	4.7	57.0	
CTX 99-74			206			14.4	38.811	0.005	15.651	0.005	18.979	0.005	14.7	74.6	
CTX 99-79	0.72522	11	62			19.6									6.7
CTX 00-132							38.655	0.005	15.610	0.004	18.917	0.004			78.8
xenoliths															
CTX 00-114	0.72675	11	19												92.8
CTX 00-115	0.70422	14	211				38.442	0.005	15.577	0.005	18.995	0.005	3.0	48.7	

* Pb isotope ratios are corrected for mass fractionation

Table 3. Cotopaxi mineral oxygen isotope data

sample name	d ¹⁸ O ₁ (per mil)	d ¹⁸ O ₂ (per mil)	d ¹⁸ O _{avg} (per mil)	std dev 2s
-------------	---	---	---	---------------

CTX 99-17

magnetite	3.02	2.48	2.75	0.54
biotite	6.47	6.63	6.55	0.16
plagioclase	7.26	7.26	7.26	0.00
glass	8.83		8.83	-
whole rock*			8.27	

CTX 99-19

magnetite	3.39	3.21	3.30	0.18
amphibole	6.37		6.37	-
plagioclase	7.33	7.16	7.25	0.17
glass	6.44	6.20	6.32	0.24
whole rock*			6.42	

CTX 99-42

biotite	6.64	6.80	6.72	0.16
plagioclase	7.33	7.54	7.44	0.21
whole rock*				

CTX 99-25

magnetite	4.10	4.00	4.05	0.10
pyroxene	6.54	6.45	6.50	0.09
plagioclase	6.60	6.68	6.64	0.08
glass	7.26	7.33	7.30	0.07
whole rock*			6.75	

Table 3, continued

sample name	d ¹⁸ O ₁ (per mil)	d ¹⁸ O ₂ (per mil)	d ¹⁸ O _{avg} (per mil)	std dev 2s
-------------	---	---	---	---------------

CTX 99-26

magnetite	4.89		4.89	-
pyroxene	6.38	6.22	6.30	0.16
plagioclase	6.49	6.65	6.57	0.16
glass	8.01	7.94	7.98	0.07
whole rock*			6.93	

CTX 00-129

magnetite	4.07	4.25	4.16	0.18
pyroxene	6.31	6.42	6.37	0.11
plagioclase	6.91	7.05	6.98	0.14
glass	7.25	7.03	7.14	0.22
whole rock*			6.85	

CTX 99-28

magnetite	5.68		5.68	-
pyroxene	6.16	6.22	6.19	0.06
plagioclase	6.63	6.53	6.58	0.10
glass	6.58		6.58	
whole rock*			6.49	

GMG II (n = 15)

Standard; Gore Mt. Garnet

5.57

0.299

*calculated from mineral percentages

1; first measurement, 2; repeat measurement, avg; average

Table A1. Electron microprobe analyses of minerals in rhyolite

sample	SiO ₂	MgO	Na ₂ O	Al ₂ O ₃	FeO	MnO	K ₂ O	CaO	TiO ₂	total	An#	Ab
Amphibole												
CTX-19	43.46	13.75	2.29	11.24	13.04	0.31	0.41	11.06	2.20	97.74		
CTX-19	43.58	13.89	2.34	11.47	13.07	0.23	0.38	11.20	2.25	98.41		
CTX-19	43.45	13.81	2.24	11.26	12.85	0.24	0.48	11.30	2.23	97.86		
CTX-19	43.87	13.60	2.19	10.90	13.77	0.34	0.41	10.97	1.72	97.78		
CTX-19	42.17	12.69	2.28	11.69	14.54	0.31	0.46	11.09	2.06	97.28		
CTX-19	43.07	13.85	2.32	11.19	12.90	0.21	0.46	11.19	2.14	97.32		
CTX-19	43.78	13.50	2.19	11.05	13.11	0.28	0.39	11.09	1.94	97.33		
CTX-19	43.75	13.65	2.16	11.31	13.02	0.16	0.43	11.09	2.14	97.71		
Biotite												
CTX-15	39.62	15.90	0.08	15.32	12.72	0.13	6.69	0.29	3.63	94.37		
CTX-15	36.54	15.82	0.19	13.88	12.34	0.19	3.04	1.59	3.33	86.92		
CTX-17	36.63	12.40	0.56	14.93	17.16	0.21	5.25	0.73	3.34	91.20		
CTX-17	37.10	12.19	0.13	15.22	16.71	0.24	7.22	0.38	3.19	92.37		
CTX-17	36.84	12.34	0.65	15.29	17.84	0.19	7.45	0.23	3.36	94.18		
CTX-19	37.47	11.74	0.22	14.53	17.60	0.23	5.59	0.43	3.43	91.25		
CTX-19	36.83	12.07	0.59	15.18	18.07	0.24	8.72	0.00	3.50	95.20		
CTX-42	38.07	14.14	0.78	16.85	13.97	0.23	7.51	0.10	3.42	95.10		
CTX-42	38.12	15.52	0.73	15.54	14.33	0.22	8.25	0.02	3.23	96.04		
CTX-42	36.81	14.62	0.78	14.94	13.81	0.22	8.18	0.12	3.19	92.71		
Plagioclase												
CTX-15	61.34	0.00	6.31	25.56	0.06	0.00	0.32	6.79	0.00	100.38	36.5	61.4
CTX-15	59.73	0.00	6.16	26.37	0.18	0.00	0.27	7.97	0.03	100.71	41.0	57.3
CTX-15	59.86	0.00	6.08	26.53	0.12	0.01	0.26	8.11	0.07	101.02	41.8	56.7
CTX-15	59.16	0.00	6.32	26.67	0.12	0.02	0.27	8.18	0.03	100.77	41.0	57.4
CTX-15	59.00	0.00	6.26	26.85	0.23	0.03	0.25	8.36	0.04	101.01	41.8	56.7
CTX-15	61.71	0.00	6.46	25.43	0.14	0.03	0.34	6.71	0.00	100.81	35.7	62.2
CTX-15	57.64	0.00	5.86	27.52	0.20	0.00	0.20	9.35	0.01	100.77	46.3	52.5
CTX-15	60.00	0.00	6.21	26.71	0.15	0.04	0.23	8.17	0.02	101.51	41.5	57.1
CTX-15	61.20	0.00	6.87	25.72	0.18	0.00	0.30	7.18	0.03	101.48	35.9	62.2
CTX-15	60.69	0.00	6.15	25.92	0.15	0.00	0.28	7.29	0.00	100.48	38.9	59.3
CTX-15	60.66	0.00	6.82	25.95	0.23	0.04	0.27	7.48	0.01	101.46	37.1	61.2
CTX-15	62.55	0.00	5.88	25.11	0.12	0.02	0.35	6.18	0.00	100.21	35.8	61.7
CTX-15	62.77	0.00	6.23	25.01	0.13	0.04	0.35	6.31	0.02	100.85	35.1	62.6
CTX-15	60.34	0.00	6.11	26.26	0.20	0.00	0.27	7.96	0.04	101.18	41.1	57.2
CTX-15	59.26	0.00	5.97	26.28	0.18	0.00	0.23	8.06	0.01	99.98	42.1	56.5
CTX-15	60.34	0.00	6.21	26.07	0.13	0.01	0.32	7.78	0.02	100.87	40.1	58.0
CTX-15	59.61	0.00	6.14	26.68	0.21	0.02	0.24	8.26	0.00	101.16	42.0	56.5
CTX-15	59.95	0.00	6.01	26.04	0.11	0.00	0.28	7.65	0.00	100.06	40.6	57.6
CTX-15	59.94	0.00	5.95	25.75	0.24	0.01	0.26	7.68	0.00	99.82	41.0	57.4
CTX-15	60.46	0.00	7.06	25.80	0.26	0.00	0.27	7.52	0.03	101.41	36.5	62.0
CTX-15	59.70	0.00	6.62	26.52	0.14	0.05	0.26	8.08	0.04	101.40	39.7	58.8
CTX-15	59.64	0.00	6.35	26.49	0.23	0.02	0.23	8.08	0.00	101.05	40.7	57.9
CTX-19	57.13	0.00	5.62	28.33	0.29	0.02	0.16	10.11	0.00	101.67	49.4	49.7
CTX-19	56.20	0.00	5.38	28.62	0.29	0.05	0.15	10.62	0.00	101.32	51.7	47.4
CTX-19	61.73	0.00	6.75	25.46	0.12	0.00	0.34	6.52	0.00	100.92	34.1	63.8
CTX-19	61.41	0.00	6.70	25.77	0.10	0.01	0.32	7.05	0.03	101.39	36.0	62.0

Table A1, Con't

sample	SiO ₂	MgO	Na ₂ O	Al ₂ O ₃	FeO	MnO	K ₂ O	CaO	TiO ₂	total	An	Ab
CTX-19	60.50	0.00	6.34	26.44	0.21	0.04	0.32	7.70	0.06	101.61	39.4	58.7
CTX-19	59.78	0.00	6.81	26.37	0.34	0.02	0.29	7.93	0.00	101.54	38.5	59.9
CTX-19	60.75	0.00	6.23	25.63	0.11	0.00	0.34	7.08	0.01	100.15	37.8	60.1
CTX-19	60.06	0.00	6.50	26.10	0.13	0.04	0.28	7.78	0.04	100.93	39.2	59.2
CTX-19	56.38	0.00	5.29	28.52	0.29	0.01	0.15	10.71	0.06	101.39	52.3	46.8
CTX-19	61.26	0.00	6.80	25.86	0.13	0.00	0.35	6.88	0.03	101.31	35.1	62.8
CTX-19	58.67	0.00	6.34	26.63	0.27	0.00	0.22	8.57	0.00	100.71	42.2	56.5
CTX-19	61.48	0.00	6.63	25.09	0.11	0.03	0.34	6.63	0.01	100.31	34.9	63.0
CTX-19	61.20	0.00	6.69	25.25	0.11	0.03	0.35	6.55	0.00	100.18	34.3	63.5
CTX-19	59.80	0.00	6.04	26.73	0.34	0.02	0.25	8.38	0.01	101.56	42.7	55.8
CTX-19	58.00	0.00	6.03	25.57	0.21	0.07	0.26	8.04	0.02	98.19	41.7	56.7
CTX-17	61.30	0.00	7.77	24.75	0.10	0.02	0.38	6.41	0.00	100.73	30.6	67.2
CTX-17	61.30	0.00	7.77	24.75	0.10	0.02	0.38	6.41	0.00	100.73	30.6	67.2
CTX-17	62.94	0.00	8.31	24.33	0.10	0.01	0.37	5.63	0.00	101.68	26.7	71.3
CTX-17	62.24	0.00	7.80	24.48	0.09	0.01	0.36	6.29	0.00	101.27	30.2	67.7
CTX-17	61.43	0.00	7.86	24.94	0.17	0.02	0.36	6.25	0.00	101.03	29.9	68.0
CTX-17	62.27	0.00	7.90	25.32	0.22	0.05	0.36	6.24	0.00	102.35	29.8	68.2
CTX-17	62.02	0.00	7.72	25.31	0.16	0.01	0.33	6.68	0.03	102.26	31.8	66.4
CTX-17	61.16	0.00	7.51	25.61	0.11	0.05	0.30	6.86	0.00	101.59	33.0	65.3
CTX-17	62.45	0.00	7.80	25.03	0.13	0.06	0.35	6.24	0.04	102.08	30.0	68.0
CTX-17	61.45	0.00	7.62	24.91	0.12	0.00	0.36	6.49	0.04	101.00	31.3	66.6
CTX-17	62.53	0.00	7.94	24.82	0.09	0.04	0.35	6.15	0.02	101.93	29.4	68.6
CTX-17	62.17	0.00	7.93	25.03	0.17	0.00	0.39	6.06	0.02	101.77	29.0	68.7
CTX-17	61.84	0.00	8.00	24.82	0.09	0.00	0.36	6.10	0.02	101.22	29.1	68.9
CTX-17	62.09	0.00	7.80	25.04	0.10	0.04	0.35	6.28	0.00	101.69	30.2	67.8
CTX-17	61.44	0.00	7.68	25.58	0.14	0.01	0.31	6.87	0.01	102.04	32.5	65.8
CTX-17	60.73	0.00	7.52	24.99	0.11	0.02	0.34	6.48	0.03	100.21	31.6	66.4
CTX-42	65.57	0.00	7.84	22.41	0.24	0.05	0.79	4.15	0.04	101.17	21.5	73.6
CTX-42	61.06	0.00	7.78	25.09	0.05	0.00	0.34	6.58	0.03	100.93	31.2	66.9
CTX-42	62.12	0.00	7.54	24.57	0.12	0.01	0.40	5.77	0.03	100.59	29.0	68.6
CTX-42	59.23	0.00	6.50	26.64	0.15	0.07	0.23	8.36	0.00	101.19	41.0	57.7
CTX-42	61.38	0.00	7.82	25.56	0.20	0.00	0.28	6.85	0.02	102.14	32.1	66.3
CTX-42	59.89	0.00	7.03	26.46	0.22	0.00	0.24	8.12	0.05	102.01	38.4	60.2
Oxides												
CTX-17	0.05	0.41	0.00	2.23	85.91	0.60	0.00	0.00	5.45	94.66		
CTX-17	0.04	0.42	0.00	2.28	85.04	0.69	0.00	0.00	5.46	93.94		
CTX-17	0.02	0.42	0.00	2.29	85.60	0.63	0.00	0.03	5.26	94.26		
CTX-17	0.02	0.40	0.00	2.19	85.37	0.59	0.00	0.02	5.38	93.97		
CTX-17	0.01	0.07	0.00	0.00	1.56	0.36	0.01	53.44	0.02	55.47		
CTX-19	0.05	1.45	0.00	2.52	83.71	0.71	0.00	0.04	5.67	94.15		
CTX-19	1.46	0.00	0.17	0.13	86.22	0.13	0.03	0.38	0.05	88.58		
CTX-19	0.04	1.29	0.00	2.39	84.07	0.78	0.00	0.00	5.71	94.27		
CTX-19	0.02	1.33	0.00	2.46	84.39	0.66	0.01	0.00	5.79	94.66		
CTX-42	0.06	1.36	0.00	0.17	52.74	1.08	0.02	0.00	42.79	98.23		
CTX-42	0.02	1.67	0.00	0.26	54.83	0.76	0.00	0.00	39.57	97.10		
CTX-15	0.10	0.11	0.00	0.01	2.26	0.24	0.04	55.01	0.12	57.89		

Table A1, Con't

sample	SiO ₂	MgO	Na ₂ O	Al ₂ O ₃	FeO	MnO	K ₂ O	CaO	TiO ₂	total	An	Ab
Pyroxene												
CTX-19	52.54	14.44	0.34	1.44	10.63	0.30	0.00	20.19	0.40	100.28		
CTX-19	51.50	15.15	0.32	3.42	8.72	0.22	0.00	19.89	0.73	99.94		
CTX-19	52.17	14.30	0.40	1.40	10.67	0.42	0.01	20.36	0.41	100.14		
Glass												
CTX-19	76.04	0.29	1.13	14.39	1.56	0.10	1.96	1.40	0.24	97.11	25.2	
CTX-42	76.64	0.05	2.26	15.39	0.55	0.01	1.86	1.82	0.09	98.65	14.1	
CTX-42	77.33	0.14	1.15	13.60	0.73	0.07	4.16	0.73	0.08	97.98	25.7	
CTX-42	77.40	0.16	1.51	13.82	1.00	0.08	3.21	1.16	0.10	98.42	21.7	
CTX-42	79.06	0.10	1.55	13.88	0.84	0.08	2.73	1.03	0.11	99.38	16.7	
CTX-42	77.00	0.20	0.08	12.97	1.19	0.08	1.54	1.13	0.45	94.65	23.3	
CTX-15	74.80	0.27	0.98	12.30	1.06	0.04	1.78	1.32	0.14	92.69	31.0	
CTX-15	72.11	0.28	3.57	13.81	1.12	0.05	2.76	1.36	0.13	95.20	31.1	
CTX-15	73.51	0.23	1.33	13.68	1.90	0.08	2.54	1.32	0.20	94.79	17.9	
CTX-15	74.76	0.29	0.83	14.03	1.06	0.05	1.76	1.30	0.20	94.27		
CTX-15	71.58	0.23	3.75	13.63	0.94	0.08	2.83	1.38	0.16	94.57		
Plagioclase												
CTX-20a	52.72	0.00	3.81	30.54	0.44	0.00	0.16	13.39	0.04	101.09	65.4	33.7
CTX-20a	54.17	0.00	4.52	29.63	0.41	0.03	0.14	11.76	0.02	100.66	58.5	40.7
CTX-20a	53.48	0.00	4.23	29.61	0.45	0.01	0.16	12.52	0.04	100.50	61.5	37.6
CTX-20a	53.24	0.00	4.20	30.13	0.37	0.01	0.15	12.63	0.03	100.78	61.9	37.2
CTX-20a	53.39	0.02	4.41	29.73	0.41	0.00	0.13	12.61	0.04	100.72	60.8	38.5
CTX-20a	59.95	0.06	4.46	24.62	0.63	0.03	0.66	7.64	0.09	98.14	46.3	48.9
CTX-20a	57.10	0.00	5.61	27.63	0.38	0.01	0.29	9.96	0.04	101.02	48.7	49.6
CTX-20a	54.39	0.02	4.57	29.70	0.53	0.01	0.18	11.89	0.00	101.30	58.4	40.6
CTX-20a	54.25	0.05	4.46	29.30	0.58	0.04	0.16	11.95	0.02	100.80	59.1	39.9
CTX-20a	54.01	0.00	4.16	29.07	0.62	0.00	0.15	12.46	0.07	100.53	61.8	37.3
CTX-25	52.8	0.01	3.70	30.87	0.70	0.02	0.10	13.70	0.04	101.97	66.8	32.6
CTX-25	58.31	0.47	5.27	24.66	1.83	0.01	0.67	9.06	0.28	100.58	46.8	49.2
CTX-25	52.45	0.02	4.12	29.90	0.52	0.01	0.16	12.99	0.00	100.17	63.0	36.1
CTX-25	52.8	0.01	3.89	30.65	0.53	0.02	0.12	13.67	0.00	101.74	65.5	33.8
CTX-25	52.87	0.04	3.84	30.62	0.52	0.03	0.09	13.54	0.07	101.62	65.8	33.7
CTX-129	57.41	0.03	5.89	26.90	0.58	0.00	0.25	9.64	0.05	100.76	46.8	51.7
CTX-129	50.38	0.00	3.03	31.96	0.57	0.04	0.06	15.06	0.04	101.15	73.1	26.6
CTX-129	50.41	0.00	3.13	31.86	0.57	0.00	0.06	14.66	0.04	100.77	71.8	27.8
CTX-129	55.06	0.00	4.87	28.89	0.45	0.02	0.14	11.45	0.09	100.99	56.1	43.1
CTX-129	53.14	0.00	4.43	28.90	0.34	0.04	0.10	12.12	0.01	99.15	59.8	39.6
CTX-129	54.20	0.01	4.39	29.60	0.49	0.05	0.12	12.31	0.04	101.20	60.4	39.0
CTX-28	51.17	0	4.417	28.241	0.625	0.008	0.193	12.2	0.065	96.92	59.7	39.1
CTX-28	54.71	0.004	4.715	28.6	0.374	0	0.242	11.34	0.029	100.01	56.2	42.3
CTX-28	49.12	0.019	2.815	31.387	0.66	0.059	0.063	15.16	0.041	99.34	74.6	25.1
CTX-28	54.17	0	4.676	28.926	0.595	0.006	0.175	11.65	0.045	100.24	57.3	41.6
CTX-28	51.1	0	3.544	30.508	0.57	0.011	0.116	13.87	0.068	99.79	67.9	31.4
CTX-28	48.34	0	2.329	32.799	0.452	0.057	0.04	16.05	0.044	100.11	79.0	20.7
CTX-28	54.71	0.003	4.736	28.715	0.651	0.003	0.213	11.58	0.045	100.68	56.7	42.0
CTX-28	51.24	0	3.516	30.92	0.479	0.017	0.15	13.92	0.008	100.25	68.0	31.1
CTX-28	53.37	0	4.318	29.513	0.492	0.023	0.184	12.43	0.043	100.41	60.7	38.2

Table A1, Con't

sample	SiO ₂	MgO	Na ₂ O	Al ₂ O ₃	FeO	MnO	K ₂ O	CaO	TiO ₂	total	An	Ab
CTX-26	53.89	0	4.347	29.683	1.257	0	0.163	12.32	0.073	101.73	60.4	38.6
CTX-26	54.51	0.012	4.571	28.953	0.527	0.02	0.195	11.74	0.004	100.54	58.0	40.9
CTX-26	53.2	0.01	4.285	30.125	0.568	0	0.143	12.44	0.038	100.83	61.1	38.1
CTX-26	49.37	0	2.618	31.881	0.606	0.004	0.037	15.41	0.025	99.96	76.3	23.5
CTX-26	51.25	0	3.319	31.029	0.646	0.057	0.062	14.3	0.036	100.69	70.2	29.5
CTX-26	54.43	0.022	4.184	29.171	0.587	0.033	0.209	11.85	0.037	100.53	60.2	38.5
CTX-26	48.5	0	2.187	33.053	0.632	0.048	0.035	16.22	0.001	100.68	80.2	19.6
CTX-26	49.32	0.01	2.843	31.631	0.59	0.009	0.1	15.24	0.06	99.81	74.3	25.1
CTX-26	48.83	0	2.848	31.867	0.629	0	0.092	15.5	0.002	99.76	74.6	24.8
CTX-26	48.09	0	2.249	32.451	0.591	0.039	0.086	16.35	0.029	99.88	79.7	19.8
CTX-26	51.68	0	3.563	30.807	0.528	0	0.11	13.94	0.005	100.64	67.9	31.4
CTX-26	50.07	0	3.147	31.297	0.63	0.013	0.102	14.31	0	99.60	71.1	28.3
CTX-26	49.53	0	2.874	32.146	0.601	0.057	0.064	15.31	0.04	100.67	71.1	28.3
CTX-26	52.14	0	3.416	31.309	0.66	0.029	0.094	14.07	0.034	101.75	69.1	30.4
CTX-75	56.16	0	5.555	28.426	0.277	0	0.144	10.34	0.055	101.013	50.3	48.9
CTX-75	51.81	0	3.978	30.424	0.571	0.035	0.108	13.73	0.059	100.738	65.2	34.2
CTX-75	55.99	0	5.263	27.818	0.841	0	0.238	10.65	0.059	100.856	52.1	46.6
CTX-75	54.57	0.028	4.817	29.111	0.75	0	0.148	11.85	0.07	101.371	57.1	42.0
CTX-75	49.61	0	2.762	31.914	0.593	0.025	0.091	15.37	0	100.379	75.1	24.4
CTX-75	55.42	0.029	4.767	28.456	0.536	0.038	0.185	11.39	0.044	100.9	56.3	42.6
CTX-75	54.34	0	4.987	28.485	0.552	0.018	0.175	11.56	0.034	100.182	55.6	43.4
CTX-75	50.29	0.007	3.238	31.422	0.538	0	0.085	14.75	0	100.332	71.2	28.3
CTX-75	53.83	0	4.54	29.739	0.326	0.026	0.135	12.65	0.023	101.273	60.2	39.1
CTX-75	53.92	0	4.52	29.362	0.458	0.039	0.129	12.37	0.043	100.907	59.7	39.5
CTX-75	53.31	0	4.654	29.812	0.464	0.03	0.132	12.25	0.021	100.714	58.8	40.4
CTX-75	53.04	0.009	3.984	29.77	0.338	0.021	0.133	12.55	0.045	99.92	63.0	36.2
CTX-75	57.21	0	5.711	27.241	0.594	0	0.28	9.997	0.069	101.105	48.4	50.0
CTX-75	54.26	0	4.894	28.455	0.36	0.025	0.166	11.68	0.024	99.869	56.3	42.7
CTX-75	53.43	0	4.631	29.593	0.596	0.037	0.151	12.36	0.085	100.912	59.1	40.1
CTX-75	68.11	0	3.586	18.853	1.246	0.034	0.399	5.514	0.384	98.125	44.2	52.0
Oxide												
CTX-75	0.723	2.497	0	3.303	79.05	0.425	0	0.558	8.593	95.248		
CTX-75	0.093	1.387	0	2.632	85.12	0.494	0	0.071	8.808	98.766		
CTX-75	2.119	0.628	0.088	1.681	79.1	0.56	0.129	0.273	12.13	96.749		
CTX-75	0.149	0.72	0	1.476	80.67	0.594	0.018	0.148	12.13	95.902		
CTX-75	0.059	1.545	0	3.476	83.69	0.429	0	0.012	8.625	97.988		
CTX-20a	0.06	3.70	0.00	4.85	76.61	0.29	0.02	0.03	8.48	94.03		
CTX-20a	0.09	3.72	0.00	4.72	76.41	0.26	0.00	0.04	8.48	93.70		
CTX-129	0.09	2.75	0.00	3.36	76.77	0.29	0.00	0.05	9.38	92.81		
CTX-25	0.133	3.33	0.00	4.29	77.26	0.31	0.00	0.00	9.12	94.51		
CTX-28	0.122	3.02	0	3.676	77.83	0.357	0.012	0.043	9.982	95.16		
CTX-26	0.055	2.901	0	3.939	81.4	0.333	0	0.031	9.144	97.88		
CTX-26	0.041	2.913	0	3.834	81.99	0.355	0.016	0.03	9.191	98.40		En
Pyroxene												
CTX-20a	52.68	25.50	0.00	4.32	16.42	0.28	0.01	1.15	0.21	100.56	73.5	71.8
CTX-20a	53.52	23.76	0.00	1.45	19.14	0.41	0.00	1.55	0.30	100.14	68.9	66.7
CTX-20a	49.44	13.33	0.52	6.10	9.33	0.23	0.00	20.54	0.54	100.03	71.8	40.0
CTX-20a	54.10	26.66	0.00	2.27	15.90	0.34	0.01	1.45	0.27	100.98	74.9	72.8
CTX-20a	50.42	14.38	0.41	5.09	8.40	0.18	0.00	20.26	0.52	99.65	75.3	42.7
CTX-20a	53.25	22.35	0.00	0.68	22.05	0.87	0.02	0.90	0.13	100.26	64.4	63.2
CTX-20a	51.57	14.60	0.39	2.45	9.24	0.26	0.00	20.52	0.62	99.66	73.8	42.3
CTX-20a	52.71	14.89	0.32	2.12	8.25	0.21	0.00	20.95	0.53	99.99	76.3	43.1

Table A1, Con't

sample	SiO ₂	MgO	Na ₂ O	Al ₂ O ₃	FeO	MnO	K ₂ O	CaO	TiO ₂	total	An	Ab
CTX-25	54.44	25.95	0.00	1.18	17.18	0.46	0.00	1.33	0.29	100.82	72.9	71.0
CTX-25	53.38	15.79	0.15	1.72	10.34	0.31	0.00	19.63	0.67	102.02	73.1	44.2
CTX-25	54.35	26.59	0.00	1.68	16.18	0.43	0.01	1.57	0.29	101.10	74.5	72.3
CTX-25	52.81	22.68	0.00	1.83	20.92	0.46	0.00	1.49	0.28	100.48	65.9	63.9
CTX-129	53.51	25.46	0.01	1.62	16.90	0.42	0.02	1.27	0.25	99.47	72.9	71.0
CTX-129	52.05	14.57	0.32	2.72	8.41	0.30	0.00	21.09	0.66	100.22	75.5	42.3
CTX-129	54.42	25.33	0.00	0.75	17.41	0.62	0.00	1.60	0.24	100.37	72.2	69.9
CTX-129	52.79	25.15	0.00	1.43	17.30	0.44	0.01	1.40	0.29	98.84	72.2	70.1
Pyroxene												
CTX-129	53.85	25.46	0.00	1.51	16.96	0.42	0.00	1.40	0.26	99.85	72.8	70.8
CTX-129	54.14	25.39	0.00	1.06	16.99	0.48	0.00	1.34	0.20	99.61	72.7	70.8
CTX-25	54.64	26.28	0.00	1.70	16.15	0.42	0.01	1.52	0.28	101.02	74.4	72.1
CTX-28	53.8	23.77	0.018	1.08	19.44	0.577	0.01	1.508	0.218	100.43	68.5	66.5
CTX-26	53.64	25.62	0.019	1.538	18.01	0.396	0	1.454	0.227	100.95	71.7	69.7
CTX-26	54.04	25.29	0	1.486	17.36	0.514	0	1.441	0.266	100.45	72.2	70.1
CTX-26	51.03	13.64	0.366	2.248	11.92	0.27	0	19.34	0.635	99.47	67.1	39.9
CTX-26	46.46	24.2	0	1.558	18.4	0.445	0	1.233	0.264	92.57	70.1	68.3
CTX-26	53.75	26.07	0	1.25	17.23	0.504	0.016	1.327	0.189	100.34	73.0	71.1
CTX-26	45.36	23.42	0.02	1.42	19.27	0.473	0.033	1.218	0.219	91.43	68.4	66.7
CTX-26	53.54	25.2	0	1.608	18.63	0.549	0.011	1.273	0.237	101.05	70.7	68.9
CTX-26	53.74	25.5	0	1.339	18.14	0.485	0	1.273	0.218	100.69	71.5	69.7
CTX-26	53.43	25.13	0	1.612	18.06	0.419	0	1.54	0.272	100.45	71.3	69.1
CTX-26	53.59	24.59	0	1.244	18.93	0.503	0.006	1.584	0.282	100.80	69.8	67.7
CTX-26	51.02	14.58	0.338	2.967	9.087	0.248	0.011	21.23	0.655	100.15	74.1	41.7
CTX-26	51.14	14.44	0.318	2.71	8.881	0.288	0.01	20.78	0.605	99.19	74.3	42.0
CTX-26	52.81	24.13	0	1.522	17.82	0.499	0	1.459	0.264	98.54	70.7	68.6
CTX-26	53.01	24.41	0.005	1.357	17.73	0.467	0	1.534	0.271	98.79	71.0	68.8
CTX-75	54.38	24.49	0	0.916	18.63	0.765	0	1.496	0.244	100.937	70.1	68.0
CTX-75	54.12	24.21	0	1.221	18.47	0.612	0	1.491	0.212	100.335	70.0	67.9
CTX-75	51.23	14.29	0.264	2.034	14.77	0.704	0.025	15.98	0.734	100.023	63.3	42.0
CTX-75	53.56	24.19	0	0.998	18.46	0.724	0.011	1.773	0.239	99.968	70.0	67.5
CTX-75	53.28	25.25	0	1.765	17.54	0.493	0.001	1.484	0.255	100.08	72.0	69.8
CTX-75	53.94	24.01	0.001	0.975	18.76	0.583	0.005	1.806	0.198	100.269	69.5	67.0
CTX-75	53.88	24.83	0	0.671	17.49	0.58	0.005	1.75	0.167	99.408	71.7	69.2
CTX-75	53.31	24.4	0.008	0.976	19.38	0.546	0.003	1.529	0.25	100.405	69.2	67.1
CTX-75	52.14	21.98	0	0.998	22.6	0.468	0	1.379	0.355	99.937	63.4	61.7
CTX-75	53.22	23.22	0.03	1.418	21.04	0.525	0.006	1.457	0.29	101.245	66.3	64.4
CTX-75	50.11	11.33	0.741	1.647	14.17	0.367	0.022	20.14	0.676	99.201	58.8	33.6
Glass												
CTX-20a	61.21	1.42	4.48	20.81	3.79	0.07	1.14	7.18	0.63	100.73		
CTX-20a	50.38	0.03	2.64	32.13	0.78	0.00	0.08	15.27	0.03	101.36		
CTX-20a	61.30	2.28	4.57	17.33	6.27	0.03	1.46	6.11	0.98	100.35		
CTX-20a	62.35	2.19	3.52	17.43	5.92	0.13	1.71	5.55	0.89	99.67		
CTX-20a	60.54	2.07	4.69	18.79	5.58	0.11	0.85	7.01	0.87	100.52		
CTX-20a	60.00	2.78	2.30	17.03	6.72	0.13	1.87	6.43	1.01	98.25		
CTX-20a	60.55	3.35	2.71	15.51	8.69	0.15	2.16	5.01	1.27	99.41		
CTX-25	63.4	2.29	1.74	17.26	6.42	0.13	2.13	5.11	0.93	99.40		

Table A1, Con't

sample	SiO ₂	MgO	Na ₂ O	Al ₂ O ₃	FeO	MnO	K ₂ O	CaO	TiO ₂	total	An	Ab
CTX-25	63.45	2.14	1.93	17.05	5.94	0.15	2.03	5.33	0.91	98.99		
CTX-25	62.23	2.23	2.16	17.07	5.69	0.15	2.32	5.08	0.87	97.82		
CTX-28	63.94	1.27	3.211	15.967	6.787	0.12	3.528	4.206	1.061	100.09		
CTX-28	64.8	1.832	4.099	15.325	6.858	0.103	1.949	5.045	1.089	101.11		
CTX-28	75.78	0.216	1.229	14.103	1.428	0.094	2.3	1.267	0.464	96.92		
CTX-75	70.32	3.016	4.083	11.947	5.214	0.186	3.124	1.742	0.515	100.151		
CTX-75	78.28	0.091	0.798	12.476	1.438	0.072	3.138	0.508	0.62	97.424		
CTX-75	77.56	0.02	2.074	11.156	2.452	0.061	2.058	0.897	0.789	97.07		
CTX-75	77.02	0.038	1.618	11.741	2.135	0.016	3.628	0.425	0.64	97.291		
CTX-75	80.82	0.01	0.271	11.342	2.099	0.019	2.389	0.425	0.658	98.083		
CTX-75	78.63	0	1.529	11.203	2.149	0.062	3.403	0.404	0.722	98.145		

¹ C; core, R; rim, I; inclusion² Mg# = Mg/(Mg+Fe)*100

Table A-2. Results of least squares modelling

starting comp.	ending comp.	plag	opx	cpx	amph	mag	biotite	quartz	apatite	total crystallization	R ²
Least evolved rhyolites to most evolved rhyolites											
CTX-43	CTX-67	-13.03			-2.40	-0.22	-2.13		0.41	17.37	0.11
CTX-15	CTX-67	-12.77			-2.48		-2.64		0.4	17.49	0.12
CTX-19	CTX-67	-10.19			-0.53	-0.38	-1.33	-3.1	0.13	15.4	0.19
Andesite to rhyolite											
CTX-20a	CTX-15	-50.66	-3.68	-21.2		-3.09			-1.95	80.58	0.89
CTX-53	CTX-15	-48.24	-11.18	-7.71	-5.09	-2.92				75.14	0.04
CTX-20a	CTX-60	-44.6	-30.4	26.34		-5.74			-5.77	60.17	0.06
CTX-28	CTX-19	-33.98	3.7	26.59	-59.45	-2.02				65.16	0.05
CTX-28	CTX-19	-45.76	-11.24	-6.52		-3.42			-0.75	67.69	0.13
Least evolved andesites to most evolved andesites											
CTX-28	CTX-26	-9.8	-2.02	-7.59		-1.15				-20.56	0
CTX-53	CTX-34b	-31.13	-7.86	-8.03		-3.48				-50.5	0.067
CTX-128	CTX-34b	-26.19	-5.23	-4.75		-3.6				-39.77	0.351
Electron probe data for mineral phases used for modelling											
	plag (rhy)	plag (and)	opx	cpx	amph	mag	biotite	quartz	apatite		
SiO ₂	60.69	55.82	52.94	50.87	49.55	0.01	36.64	100	0.00		
TiO ₂	0.00	0.09	0.37	0.79	0.91	17.41	2.99		0.00		
Al ₂ O ₃	25.92	27.35	1.39	2.66	6.67	1.24	17.59		0.00		
FeOt	0.15	0.68	19.65	14.49	14.97	80.63	26.22		0.28		
MgO	0.00	0.04	23.60	13.98	13.77	0.63	6.28		0.58		
CaO	6.15	10.27	2.00	16.60	12.48	0.08	0.00		60.59		
Na ₂ O	7.29	5.35	0.05	0.61	1.10	0.00	0.43		0.00		